eNeuro

Research Article: New Research | Sensory and Motor Systems

Involvement of brain-enriched guanylate kinase-associated protein (BEGAIN) in chronic pain after peripheral nerve injury

BEGAIN is a novel chronic pain-related protein

Tayo Katano[1], Masafumi Fukuda[2], Hidemasa Furue[3], Maya Yamazaki[4,5], Manabu Abe[4], Masahiko Watanabe[6], Kazuhiko Nishida[1], Ikuko Yao[1,7], Akihiro Yamada[3], Yutaka Hata[8], Nobuaki Okumura[9], Takanobu Nakazawa[10], Tadashi Yamamoto[11], Kenji Sakimura[4], Toshifumi Takao[2] and Seiji Ito[1]

[1]*Department of Medical Chemistry, Kansai Medical University, Hirakata 573-1010, Japan*

[2]*Laboratory of Protein Profiling and Functional Proteomics, Institute for Protein Research, Osaka University, Suita 565-0871, Japan*

[3]*Division of Neural Signaling, Department of Information Physiology, National Institute for Physiological Sciences, Okazaki 444-8787, Japan*

[4]*Department of Cellular Neurobiology, Brain Research Institute, Niigata University, Niigata 951-8585, Japan*

[5]*Department of Neurology, University of California, San Francisco 94158, USA*

[6]*Department of Anatomy, Hokkaido University School of Medicine, Sapporo 060-8638, Japan*

[7]*Department of Optical Imaging, Institute for Medical Photonics Research, Preeminent Medical Photonics Education & Research Center, Hamamatsu University School of Medicine, Hamamatsu, 431-3192, Japan*

[8]*Department of Medical Biochemistry, Graduate School of Medicine, Tokyo Medical and Dental University, Tokyo 113-8519, Japan*

[9]*Laboratory of Homeostatic Integration, Institute for Protein Research, Osaka University, Suita 565-0871, Japan*

[10]*Drug Innovation Center, Graduate School of Pharmaceutical Science, Osaka University, Suita, 565-0871, Japan*

[11]*Cell Signal Unit, Okinawa Institute of Science and Technology Graduate University, Okinawa 904-0495, Japan*

DOI: 10.1523/ENEURO.0110-16.2016

Received: 2 May 2016

Revised: 1 October 2016

Accepted: 4 October 2016

Published: 6 October 2016

Author Contributions: TK and SI Designed research; TK, MF, HF, AY, MY, MA, and MW Performed research; YH, NO, TN, TY, KS, and TT Contributed unpublished reagents/ analytic tools; TK, MF, HF, AY, KN and IY; Analyzed data, TK, MF, and HF Wrote the paper.

Conflict of Interest: Authors report no conflict of interest.

Correspondence: Dr. Tayo Katano, Department of Medical Chemistry, Kansai Medical University, Hirakata, 573-1010, Japan. Tel: +81-72-804-2340; Fax: +81-72-804-2349; E-mail: katanot@hirakata.kmu.ac.jp

Cite as: eNeuro 2016; 10.1523/ENEURO.0110-16.2016

1. Manuscript Title:

Involvement of brain-enriched guanylate kinase-associated protein (BEGAIN) in chronic pain after peripheral nerve injury

2. Abbreviated Title:

BEGAIN is a novel chronic pain-related protein

3. List all Author Names and Affiliations

Tayo Katano,[1] Masafumi Fukuda,[2] Hidemasa Furue,[3] Maya Yamazaki,[4, 5] Manabu Abe,[4] Masahiko Watanabe,[6] Kazuhiko Nishida,[1] Ikuko Yao,[1, 7] Akihiro Yamada,[3] Yutaka Hata,[8] Nobuaki Okumura,[9] Takanobu Nakazawa,[10] Tadashi Yamamoto,[11] Kenji Sakimura,[4] Toshifumi Takao,[2] and Seiji Ito[1]

[1]Department of Medical Chemistry, Kansai Medical University, Hirakata 573-1010, Japan

[2]Laboratory of Protein Profiling and Functional Proteomics, Institute for Protein Research, Osaka University, Suita 565-0871, Japan

[3] Division of Neural Signaling, Department of Information Physiology, National Institute for Physiological Sciences, Okazaki 444-8787, Japan

[4]Department of Cellular Neurobiology, Brain Research Institute, Niigata University, Niigata 951-8585, Japan

[5]Department of Neurology, University of California, San Francisco 94158, USA

[6]Department of Anatomy, Hokkaido University School of Medicine, Sapporo 060-8638, Japan

[7]Department of Optical Imaging, Institute for Medical Photonics Research, Preeminent Medical Photonics Education & Research Center, Hamamatsu University School of Medicine, Hamamatsu, 431-3192, Japan

[8]Department of Medical Biochemistry, Graduate School of Medicine, Tokyo Medical and Dental University, Tokyo 113-8519, Japan

[9]Laboratory of Homeostatic Integration, Institute for Protein Research, Osaka University, Suita 565-0871, Japan

[10]Drug Innovation Center, Graduate School of Pharmaceutical Science, Osaka University, Suita, 565-0871, Japan

[11]Cell Signal Unit, Okinawa Institute of Science and Technology Graduate University, Okinawa 904-0495, Japan

4. Author Contributions: TK and SI Designed research; TK, MF, HF, AY, MY, MA, and MW Performed research; YH, NO, TN, TY, KS, and TT Contributed unpublished reagents/ analytic tools; TK, MF, HF, AY, KN and IY; Analyzed data, TK, MF, and HF Wrote the paper.

5. Correspondence: Dr. Tayo Katano, Department of Medical Chemistry, Kansai Medical University, Hirakata, 573-1010, Japan. Tel: +81-72-804-2340; Fax: +81-72-804-2349; E-mail: katanot@hirakata.kmu.ac.jp

6. Number of Figures: 7 (Number of Source data: 3)

7. Number of Tables: 3 (Number of Source data: 2)

8. Number of Multimedia: 0

9. Number of words for Abstract: 250

10. Number of words for Significance Statement: 120

11. Number of words for Introduction: 622

12. Number of words for Discussion: 1328

13. Acknowledgements： We wish to thank Comprehensive Brain Science Network (CBSC) for support about the generation of floxed-mouse and antibodies against BEGAIN. This work was supported by JSPS KAKENHI Grant Numbers 23790651, 25460729, 20022040.

14. Conflict of Interest: No (State ‘Authors report no conflict of interest’)

15. Funding sources:

Abstract

Maintenance of neuropathic pain caused by peripheral nerve injury crucially depends on the phosphorylation of GluN2B, a subunit of the NMDA receptor, at its Tyr1472 (Y1472) and subsequent formation of a postsynaptic density (PSD) complex of superficial spinal dorsal horn neurons. Here we took advantage of comparative proteomic analysis based on isobaric stable isotope tags (iTRAQ) between wild-type and knockin mice with a mutation of Y1472 to Phe of GluN2B (Y1472F-KI) to search for PSD proteins in the spinal dorsal horn that mediate the signaling downstream of phosphorylated Y1472 GluN2B. Among several candidate proteins, we focused on brain-enriched guanylate kinase-associated protein (BEGAIN), which was specifically up-regulated in wild-type mice after spared nerve injury (SNI). Immunohistochemical analysis using generated antibody demonstrated that BEGAIN was highly localized at the synapse of inner lamina II in the spinal dorsal horn and that its expression was up-regulated after SNI in wild-type, but not in Y1472F-KI, mice. In addition, alteration of the kinetics of evoked EPSCs for NMDA but not those for AMPA receptors in spinal lamina II was demonstrated by BEGAIN deletion. We demonstrated that mechanical allodynia, a condition of abnormal pain induced by innocuous stimuli, in the SNI model was significantly attenuated in BEGAIN-deficient mice. However, there was no significant difference between naive wild-type and BEGAIN-knockout mice in terms of physiological threshold for mechanical stimuli. These results suggest that BEGAIN was involved in

pathological pain transmission through NMDA receptor activation by the phosphorylation of GluN2B at its Y1472 in spinal inner lamina II.

Significance Statement

We for the first time revealed that brain-enriched guanylate kinase-associated protein (BEGAIN) plays a crucial role in pathological but not physiological pain. We previously demonstrated that neuropathic pain was attenuated in knockin mice with Y1472F of GluN2B (Y1472F-KI). Here, by proteomic analysis of spinal dorsal horn, we found that the level of BEGAIN protein was increased in wild-type, but not in Y1472F-KI, mice after peripheral nerve injury. BEGAIN was localized at synapses in lamina IIi of the spinal dorsal horn. Moreover, neuropathic pain was significantly attenuated in the knockout mice of BEGAIN after peripheral nerve injury, demonstrating that BEGAIN was involved in pathological pain transmission through NMDAR activation following the phosphorylation of GluN2B at its Y1472 in spinal lamina II.

Introduction

Neuropathic pain is assumed to result from pathological neural plasticity caused by peripheral nerve injury. The pathological condition is accompanied by long-lasting abnormal pain, such as hyperalgesia or allodynia, which is maintained by multiple postsynaptic density (PSD) proteins in several areas of the brain and in spinal dorsal horn neurons. The superficial dorsal horn such as laminae I-II predominantly receives nociceptive inputs via primary afferent Aδ and C fibers; whereas low-threshold information targets deeper laminae (Todd, 2010, Braz et al., 2014). In the case of neuropathic pain, however, innocuous stimuli-triggered nociceptive pain is mediated by an abnormal pain circuit of the spinal dorsal horn, which is engaged in alteration of synaptic efficacy of interneurons in laminae IIi-IV, such as disruption of inhibitory control or facilitation of excitatory control (Braz et al., 2014, Duan et al., 2014, Peirs et al., 2015).

PSD proteins including NMDA receptors (NMDARs) and scaffold proteins participate in not only physiological pain but also abnormal pain transmission through the activation of intracellular signaling cascades in the spinal dorsal horn and brain (Craven and Bredt, 1998, Garner et al., 2000, Luo et al., 2014). The difference between physiological and pathological conditions of sensory transmission is determined by reversible change of the composition of PSD complexes in the spinal dorsal horn (Katano et al., 2008). The interaction between PSD-95 and GluN2B is accelerated after peripheral nerve injury (Peng et al., 2013). Also, a disruption of the PSD complex, such

as the interaction between PSD-95 and GluN2B attenuates neuropathic and inflammatory pain (Tao et al., 2001, Tao et al., 2003, D'Mello et al., 2011). These lines of evidence indicate that clarification of the alteration of proteins in the PSD complex is necessary for the elucidation of abnormal pain mechanisms as well as for drug discovery. However, with respect to neuropathic pain such alteration in the spinal dorsal horn has so far not been fully reported.

Phosphorylation of GluN2B at its Tyr1472 (Y1472) is crucial for maintenance of neuropathic pain in the spinal dorsal horn. The phosphorylation of GluN2B is increased in the spinal dorsal horn after peripheral nerve injury, which signal affects the localization of NMDARs containing GluN2B at the synapse and calcium influx via the receptor. On the other hand, inhibition of GluN2B phosphorylation in Fyn knockout mice or in knock-in mice with their Y1472 site of GluN2B mutated to phenylalanine (Y1472F-KI) affects the localization of GluN2B at the center of the postsynapse and that of several calcium signaling proteins, thereby attenuating mechanical allodynia (Abe et al., 2005, Nakazawa et al., 2006, Matsumura et al., 2010, Katano et al., 2011). Furthermore, neural plasticity, long-term potentiation, and fear-related learning are also impaired in Y1472F-KI mice (Nakazawa et al., 2006), suggesting that the phosphorylation of GluN2B at this site is indispensable for the neural plasticity involved in the maintenance of neuropathic pain and formation of learning and memory. However, it remains unclear how PSD proteins maintain allodynia following the phosphorylation of GluN2B

in the spinal dorsal horn, because many of the roles and functions of these proteins have not yet been identified.

Here, to identify novel proteins involved in the signaling cascades downstream of GluN2B phosphorylation at Y1472 with respect to neuropathic pain, we took advantage of proteomic screening of wild-type and Y1472F-KI mice before and after spared nerve injury (SNI). From these analyses, we identified brain-enriched guanylate kinase-associated protein (BEGAIN) as a neuropathic pain-related protein, which was specifically expressed in the spinal lamina IIi. This study is the first report on the role of BEGAIN in abnormal pain sensations after peripheral nerve injury *in vivo*. A part of the data in this paper has already been presented in abstract form at Society for Neuroscience meetings (Katano et al., 2012, 2015).

Materials and Methods

Animals and behavioral studies

GluN2B Y1472F-KI mice were produced by a gene-targeting technique as reported previously (Nakazawa et al., 2006). BEGAIN-floxed ($BEGAIN^{flox/+}$) mice were produced by using the embryonic stem (ES) cell line RENKA, which was derived from the C57BL/6N strain (Mishina and Sakimura, 2007). Homologous recombinants among the ES cells were identified by Southern blot analysis. To yield heterozygous knockout ($BEGAIN^{+/-}$) mice, $BEGAIN^{flox/+}$ mice were crossed with TLCN-Cre mice, by which recombination is induced throughout the whole body (Nakamura et al., 2001, Mishina and Sakimura, 2007).

The neuropathic pain model of SNI was made according to the procedure reported previously (Decosterd and Woolf, 2000) with a slight modification (Katano et al., 2011). In the behavioral study, mice were randomly placed individually in a plastic case, which was placed on a mesh floor or plantar plate. Before each test, the mice were habituated for 0.5-1 h to allow acclimatization to the test environment. Mechanical threshold or allodynia elicited by SNI was assessed by use of the von Frey test. Each test was started from an initial filament (0.008 g). The filaments were inserted through the mesh floor of the cage and applied in an ascending order 5 times at an interval of a few seconds to the plantar surface of the hindpaw ipsilateral to the operation side. The threshold was taken as the lowest force required for a withdrawal reflex of the paw to 1 of 5 repetitive stimuli with the cut-off set at 2 g (Tal and Bennett, 1994, Decosterd and Woolf, 2000).

Following Chaplan's up-down methods, the threshold was further confirmed by additional tests showing the positive and negative responses by using upper and lower filaments, respectively (Chaplan et al., 1994).

Antibodies

Rabbit anti-BEGAIN C17 and goat anti-PKCγ C14 antibodies were raised against C-terminal peptide SRKDSLTKAQLYGTLLN of mouse BEGAIN and mouse PKCγ (Yoshida et al., 2006), respectively. Commercially available antibodies against PSD-95 (Upstate Biotech.), Hsp60 (Upstate Biotech.), GluN2B (Millipore), synaptophysin (Millipore), glial fibrillary acidic protein (GFAP, Millipore), β-tubulin (Sigma-Aldrich), and isothiocyanate-conjugated *Bandeiraea simplicifolia* isolectin B4 (IB4, Sigma) from the sources indicated were also used.

Drug administration

Intrathecal (*i.t.*) injection was performed as described previously (Minami et al., 1995). A 27-gauge stainless-steel needle (0.35 mm, o.d.) attached to a micro-syringe was inserted between the L5 and L6 vertebrae of conscious mice, and Ro25-6981 (100 μg/mouse, Tocris; (Mihara et al., 2011, Kim et al., 2012) in 1% DMSO/saline (5 μl) was injected *i.t.* 0.5 h before assessment of mechanical allodynia. Attenuation of the withdrawal threshold for mechanical allodynia by Ro25-6981, which is a specific

antagonist of NMDAR containing GluN2B was measured 3 times between 30 and 90 min after the injection.

Subcellular fractionation of spinal dorsal horn for Western blotting

After anesthesia with isoflurane, the spinal dorsal horn at L4-L6 levels was collected and homogenized with a Potter-Elvehjem homogenizer in 20 mM Tris-HCl (pH 8.0) containing 0.32 M sucrose, 2 mM DTT, protease inhibitor cocktail (Sigma-Aldrich), and phosphatase inhibitor (Nacalai Tesque). After centrifugation of the homogenate at 800 x g for 10 min, the pellet (P1; nuclear) and supernatant (S1) were separated. The S1 fraction was then centrifuged at 13,800 x g for 20 min. The precipitate (P2), the membrane fraction, was suspended in 20 mM Tris-HCl (pH 8.0), after which an equal volume of 1% Triton X-100 in 20 mM Tris-HCl (pH 8.0) was added to it. The membrane fraction was rotated for 15 min at 4 ˚C and then centrifuged for 20 min at 15,000 rpm. The resulting pellet was used as the crude PSD fraction (cPSD).

Preparation of PSD fractions from spinal dorsal horn for proteomic analysis

After anesthesia with isoflurane, more than 100 male 8-10 week-old mice from 4 groups comprising wild-type naive, wild-type SNI at day 7, Y1472F-KI naive, and Y1472F-KI SNI at day 7 were killed, and their lumbar spinal dorsal horn at L4–L6 levels was collected. The PSD fraction was prepared, essentially as described by Carlin et al. (1980) with slight modifications (Carlin et al., 1980). For preparation of PSD fractions,

lumbar spinal dorsal horns were homogenized in solution A (0.32 M sucrose, 1 mM $NaHCO_3$, 1 mM $MgCl_2$, 0.5 mM $CaCl_2$, 1 mM Na_3VO_4, and protease inhibitor cocktail (Sigma)) with a Potter-Elvehjem homogenizer. The pellet obtained by centrifugation of the S1 fraction at 13,800 x g for 20 min was used as the P2 fraction. This fraction was then suspended in solution B (0.32 M sucrose containing 1 mM $NaHCO_3$) and applied onto a discontinuous sucrose gradients composed of 3.4 ml of 1.2 M, 3.4 ml of 1.0 M, and 3 ml of 0.85 M sucrose in 1 mM $NaHCO_3$ in tubes; and the tube was subsequently centrifuged at 82,500 x g for 120 min. The interface between 1.0 and 1.2 M sucrose was collected and dissolved for 15 min with buffer C consisting of 0.5% TritonX-100 and 6 mM Tris-HCl (pH 8.0). For collection of the insoluble fraction, the interface fraction was centrifuged at 32,800 x g for 30 min. The insoluble fraction was dissolved in 7 M urea, 2 M thiourea, 4% CHAPS, and 2% SDS and used as the PSD fraction (PSD). The purity of the PSD fraction was confirmed by Western blotting with anti-PSD-95 and anti-Hsp60 antibodies.

Western blot analysis

In each figure, all subcellular fractions or homogenates from different tissues were subjected to a single gel for SDS-PAGE (10 or 12.5% acrylamide); and the separated proteins were transferred to a PVDF membrane. After blocking for 1 h at room temperature with 3% skimmed milk or 3% BSA in TBS-T buffer consisting of 0.1% Triton X-100, 150 mM NaCl, and 10 mM Tris-HCl (pH 7.5), the membrane was

234 incubated at 4 °C overnight with rabbit anti-BEGAIN (0.5 μg/ml), anti-PSD-95 (1:1000),
235 anti-Hsp60 (1:1000) or anti-β-tubulin (1:2000) antibodies. The membrane was then
236 washed with the TBS-T buffer and incubated for 1 h with horseradish
237 peroxidase-conjugated goat anti-rabbit IgG (1:20,000; Zymed) or goat anti-mouse IgG
238 (1:20,000; GE Healthcare). It was then washed 4 times with the TBS-T buffer. The
239 immunoreactivity was detected by use of an enhanced chemiluminescence detection kit
240 (Chemi-Lumi One Super, Nacalai Tesque) after incubation with horseradish
241 peroxidase-conjugated goat anti-rabbit IgG (1:20,000; Zymed) or goat anti-mouse IgG
242 (1:20,000; GE Healthcare). Detection of several proteins, such as BEGAIN, PSD-95,
243 Hsp60, GluN2B and beta-tubulin in a single gel was performed sequentially. That is,
244 the preceding antibody was stripped from the PVDF membrane, which was then
245 re-probed with another primary antibody for the detection of next protein.
246
247 **In gel digestion and iTRAQ labeling**
248 PSD fractions (25 μg) prepared from the 4 groups were separated on 10%
249 SDS-PAGE gels without stacking gel; and after CBB staining the lanes were separated
250 into 6 parts according to molecular-weight range: molecular weights higher than 250,
251 between 250 and 150, 150 and 100, 100 and 75, 75 and 50, and lower than 50 kDa.
252 In-gel digestion was performed for the PSD proteins in these 24 gel parts in individual
253 tubes by using 10 mM dithiothreitol for reduction, 100 mM acrylamide for alkylation,
254 500 nM trypsin for digestion and 500 mM triethylammonium bicarbonate (TEAB) as the

buffer for all the reactions. Tryptic peptides were extracted from the gel pieces with 50% acetonitrile (ACN) in 0.1% trifluoroacetic acid (TFA) and lyophilized. Digested samples were labeled with the isobaric stable isotope tags (114-, 115-, 116-, and 117-iTRAQ reagents) for comparative quantitation according to the manufacturer's instruction (Applied Biosystems). The 4 iTRAQ-labeled samples with the same molecular weight range were combined after having been diluted 10 times with 10 mM KH_2PO_4 (pH 3.0) in 25% ACN. The combined sample was purified by cation-exchange chromatography (cartridge column kit, Applied Biosystems), followed by desalting with a Bond Elut C18 cartridge column (Agilent Technologies). The eluate was dried by vacuum centrifugation, dissolved in 0.1% TFA in 50% ACN, and diluted 10 times with 0.1% TFA for further analysis.

LC-MALDI-MS and MS/MS analysis

The combined samples were applied to a Prominence nano-LC System (Shimadzu) coupled to an AccuSpot LC spotting system (Shimadzu). The mobile phases were solvent A (0.1% TFA in water/ACN [95:5, v/v]) and B (0.1% TFA in water/ACN [10:90, v/v]). Peptide digests were adsorbed and desalted on a precolumn (Monolith, 0.2 mm×100 mm; (Kyoto Monotech Co. Ltd.)) with 0.1% TFA in water at a flow rate of 35 µL/min (0–5 min). Peptide digests were then separated on an analytical column (Monolith, 0.1 mm×250 mm) at a flow rate of 1 µl/min with a gradient obtained by changing the ratio of solvent B (%) as follows: 5 min, 10% (initial %); 7 min, 10%; 10

min, 15%, 36 min, 40%; 40 min, 60%; 41 min, 95%; 59 min, 95%; 60 min, 10%; 77 min, 10%. The eluate was recorded at 210 nm, mixed with MALDI (matrix-assisted laser desorption ionization) matrix solution (5 mg/ml α-cyano-4-hydroxycinnamic acid [CHCA] in 60% [v/v] ACN containing 0.1% TFA), and then directly spotted onto a 192-well MALDI plate (Applied Biosystems). MS and MS/MS analyses were performed on a 4700 Proteomics Analyzer (Applied Biosystems).

Identification and quantitative analysis

All MS/MS spectra were combined, processed, database-searched, and subjected to comparative quantification with ProteinPilot™ software (version 2.0.1, Applied Biosystems), in which the paragon algorithm is used to carry out database matching for protein identification based on a novel small sequence tag search method with simple search criteria (Shilov et al., 2007). For identification, "Gel-based ID" was selected in the software with propionamide for Cys alkylation. The UniProt protein database, which had been downloaded (March 2009) from a website and updated on a regular basis, was used for database searching. In order to demonstrate search results, we adopted the identified that showed more than 95%-confidence identification (Paragon™ Algorithm) based on their MS/MS spectra and had a low false-discovery rate (FDR <1.0 %). For scoring, the MS/MS spectra that have not already been used to justify an already assigned more confident protein only contributed to the "Unused ProtScore." Therefore, identified proteins were only reported if they had a sufficient Unused

297 ProtScore as top hit removing redundant proteins entries. Bias correction was
298 performed by using ProteinPilot^{TM} software as normalization for comparative
299 quantification to correct the median ratio to unity, based on the assumption that most
300 proteins do not change in expression. Namely, the observed iTRAQ ratios of each
301 peptide were divided by the corresponding median values of the iTRAQ ratios so that
302 unequal mixing of the different labeled samples could be corrected. Identified proteins
303 with iTRAQ ratios below the low range (0.8) and *p*-value of < 0.05 were considered to be
304 underexpressed, whereas those above the high range (1.2) and *P*-value of < 0.05 were
305 considered to be overexpressed when compared with those of the naive group. For
306 evaluation of the expression level, some proteins extracted from two or more different gel
307 parts of molecular range were excluded. The mass spectrometry proteomics data were
308 deposited to the Peptide Atlas (http://www.peptideatlas.org) with the dataset identifier,
309 PASS00929.
310
311 **Histochemistry**
312 Animals were anesthetized by an intraperitoneal administration of sodium
313 pentobarbital (50 mg/kg) and perfused with 4% paraformaldehyde in 0.12 M sodium
314 phosphate (pH 7.4). Following dissection, spinal cords were postfixed for 4 h in the
315 same fixative at 4 ˚C and then cryoprotected overnight in 30% (w/v) sucrose in PBS (-) at
316 pH 7.4. Transverse sections (14-μm thick) of the spinal cord at L4-L6 were cut on a
317 cryostat and processed for immunohistochemistry with anti-BEGAIN (1 μg/ml),

anti-PKCγ (1 μg/ml), anti-PSD-95 (1 μg/ml), anti-synaptophysin (1:1000) or anti-GFAP (1:500) as primary antibody for overnight at 4 ˚C after antigen retrieval at 110 ˚C for 15 min in citrate buffer (pH 6.0). Thereafter the sections were incubated with Alexa 488-, 546- or 633-conjugated goat anti-mouse, -rabbit or -goat IgG as secondary antibody (1:300-500, Invitrogen) for 90 min at room temperature. For the fluorescein IB4 staining condition, sections of spinal cords were preincubated for 20 min at room temperature with 0.1% Triton-X 100 in PBS supplemented with 0.1 mM $CaCl_2$, 0.1 mM $MgCl_2$, and 0.1 mM $MnCl_2$ following antigen retrieval. Then, the sections were incubated with 50 μg/ml of IB4 and anti-BEGAIN overnight at 4°C in above preincubaation buffer containing 2% BSA. Fluorescence images were captured with a Zeiss laser scanning confocal microscope (LSM700), and quantification of fluorescent signals was carried out by use of ImageJ software. The co-localization analysis was performed by use of Imaris (BITPLANE) (Costes et al., 2004, Marvizon et al., 2007). The z-series fluorescence images were captured and 3D data of region of interest were automatically analyzed after threshold setting. The threshold was defined using 2D histogram and Preview window in Imaris Coloc, which helps distinguish between low intensity colocalization pixels of synaptic proteins and background (Costes et al., 2004). In the 2D histogram, we choose pixels closest to the diagonal line. The statistical validity of colocalization was quantified by computing the Manders' overlap coefficient analysis.

Reverse transcriptional PCR for BEGAIN

The expression level of BEGAIN was determined in the spinal dorsal horn, dorsal root ganglion (DRG), and brain by performing reverse transcription–polymerase chain reaction (RT-PCR) analysis. Total RNA was extracted by use of Trizol according to the manufacturer's protocol (Invitrogen). First-strand cDNA for each tissue as a template was synthesized with Revatra Ace and oligo dT_{20}. BEGAIN was detected by RT-PCR using primers (forward, ATTGACAAGCTGTCGGAGGA; and reverse, GGCAGCTCGGACACCTTAT).

Electrophysiology

The electrophysiological recordings used for the current experiments were similar to those in an earlier study (Uta et al., 2010). Briefly, a 500-µm thick transverse slice of mouse spinal cord was prepared 7 days after SNI and set in a chamber perfused with Krebs solution (in mM: NaCl 117, KCl 3.6, $CaCl_2$ 2.5, $MgCl_2$ 1.2, NaH_2PO_4 1.2, $NaHCO_3$ 25, and glucose 11) equilibrated with 95% O_2-5% CO_2 at 36 °C. Patch-pipettes were filled with a solution having the following composition (in mM): Cs_2SO_4, 110; tetraethylammonium, 5; $CaCl_2$, 0.5; $MgCl_2$, 2; EGTA, 5; Mg-ATP, 5; HEPES, 5; (pH 7.2 adjusted with CsOH). The pipettes had a resistance of 8-12 MΩ. Blind whole-cell voltage-clamp recordings were obtained from substantia gelatinosa (SG, lamina II) neurons. A monopolar stimulating electrode was put on the surface of the slice near the recording neuron to elicit evoked EPSCs. Drugs were dissolved in Krebs

360 solution and applied by bath-application.

361

362 **Statistics**

363 Data for immunohistochemistry and mechanical allodynia were expressed as the
364 mean ± SEM and analyzed by using the unpaired *t*-test, Mann-Whiteney U-test or
365 repeated ANOVA followed by the Bonferroni *post hoc* test. $p < 0.05$ was considered to
366 be statistically significant. Co-localization of synaptic proteins was quantified by
367 Manders' overlap coefficient analysis. Electrophysiological data were expressed as the
368 mean ± SEM. Statistical significance was determined as $p < 0.05$ by using the paired
369 t-test.

Results

Attenuation of mechanical allodynia by lumbar intrathecal injection of Ro 25-6981, an antagonist of GluN2B-NMDAR, and in Y1472F-KI mice after SNI

We previously demonstrated that phosphorylation of GluN2B at its Y1472 was increased in the spinal dorsal horn of wild-type mice after spinal nerve transection (SNT) and SNI (Matsumura et al., 2010, Katano et al., 2011) and that mechanical allodynia after the operations was significantly attenuated in Y1472F-KI mice. To clarify the participation of NMDAR activity of the spinal dorsal horn in neuropathic pain following the phosphorylation of its GluN2B subunit at Y1472, we prepared SNI-operated wild-type mice with or without *i.t.* injection of the GluN2B-specific antagonist Ro25-6981 into their lumbar spinal cord and SNI-operated Y1472F-KI mice, and analyzed their responses to mechanical stimulation (Fig. 1A). Seven days after SNI, the paw withdrawal threshold for the wild-type mice drastically dropped (0.19 ± 0.07 g, n=12) compared with that for the naive mice (1.21 ± 0.12 g, n = 12). Ro25-6981 significantly attenuated the decrease in the threshold within 30-90 min after *i.t.* injection into the wild-type mice (0.73 ± 0.12 g, n = 12). Furthermore, the decrease in the withdrawal threshold for Y1472F-KI mice after SNI (0.82 ± 0.12 g, n = 12) was also partially attenuated compared with that for the wild-type mice after SNI. These results confirmed that the phosphorylation of GluN2B at Y1472 in the spinal dorsal horn was important for the maintenance of neuropathic pain even 7 days after SNI. Therefore we chose the spinal dorsal horn as the target tissues for our proteomic analysis.

Identification and quantitative analysis of PSD proteins in the spinal dorsal horn by proteomic analysis using isobaric stable isotope tags (iTRAQ)

To investigate the molecular mechanism of central sensitization via the phosphorylation of GluN2B in the spinal dorsal horn, we searched for novel proteins involved in neuropathic pain by comparative analysis using the proteomic approach. We chose the spinal dorsal horn as target tissues for proteomic approach, because mechanical allodynia caused by SNI was attenuated by intrathecal injection of Ro25-6981, a selective blocker of NMDAR containing GluN2B, into the lumbar spinal cord (Fig. 1A). Differential analysis of the lumbar spinal dorsal horn among 4 groups, i.e., wild-type naive, wild-type SNI, Y1472F-KI naive, and Y1472F-KI SNI was performed by using the proteomic approach. We purified the PSD fraction of the lumbar spinal dorsal horn from more than 100 mice in each group by sucrose-density gradient. The purity was confirmed by Western blotting with anti-PSD-95 and Hsp60 antibodies, which labeled the PSD and mitochondrial fraction, respectively (Fig. 1B). Each PSD fraction was solubilized and separated by molecular size-dependent fractionation using SDS-PAGE (Fig. 1C, 6 pieces of gels from a given lane). The tryptic peptides derived from PSD proteins in 6 corresponding gel pieces from each group were labeled with 4-plex iTRAQ reagents (114, wild-type naive; 115, wild-type SNI; 116, Y1472F-KI naive; and 117, Y1472F-KI SNI). MS/MS spectra of the labeled peptides were processed and database-searched with ProteinPilot™ software, and protein amounts

412 were quantified based on labeled iTRAQ peaks. Particularly, we used peptides with
413 more than 95%-confidence and FDR < 1% for protein identification. By using these
414 criteria, 208 and 63 proteins including receptors, channels, kinases, and scaffold proteins
415 were identified from single and multiple gel pieces, respectively (Fig. 1C and PASS00929
416 in Peptide Atlas). For quantitative analysis, the median was used for normalization of
417 the iTRAQ ratios as described in "Materials and Methods." The level of 2 proteins,
418 Ras/Rap GTPase-activating protein SynGAP and Protein piccolo was increased in both
419 wild-type and Y1472F-KI mice after SNI (Table 1 and PASS00929 in Peptide Atlas).
420 These proteins were identified as neuropathic pain-related proteins independent of
421 GluN2B phosphorylation at Y1472. Moreover, we specifically demonstrated that
422 increased expression of 2 proteins (IQ motif and SEC7 domain-containing protein 2, SH3
423 and multiple ankyrin repeat domains protein 2) and decreased expression of 2 proteins
424 (Actin cytoplasmic 2, Voltage-dependent anion-selective channel protein 1) in
425 Y1472F-KI mice after SNI compared with their expression in naive mice, and thus their
426 levels were affected by the attenuation of GluN2B phosphorylation at Y1472 after SNI.
427 Thirteen up-regulated proteins including CaMKII and 2 down-regulated proteins,
428 pyruvate dehydrogenase E1 component subunit beta and D-beta-hydroxybutyrate
429 dehydrogenase, were found only in the wild-type SNI group (Fig. 1C, Table 1 and
430 PASS00929 in Peptide Atlas). Among these former proteins, one of them, i.e., BEGAIN,
431 was reported to interact with PSD-95 in the brain; however, its molecular function in the
432 brain and spinal cord have not yet be reported. Here, we focused on BEGAIN, whose

expression was increased (1.34 fold vs. wild-type naive, Table 1) in wild-type mice, but not in Y1472F-KI mice, after SNI.

Difference in protein expression of BEGAIN in the spinal dorsal horn after SNI between wild-type and Y1472F-KI mice

In the proteomic analysis, we identified BEGAIN, CaMKII and others, whose expression was specifically increased in the PSD fraction of the spinal dorsal horn of the wild-type SNI mice. The amount and posttranslational modification of CaMKII and other proteins in the superficial spinal dorsal horn are increased after nerve injury (Katano et al., 2008, Peng et al., 2013). Thus, to further confirm the relative abundance and localization of BEGAIN in the spinal cord, we determined its expression by immunohistochemistry using anti-BEGAIN antibody generated in this study. The fluorescence intensity of BEGAIN signals significantly increased in the superficial dorsal horn of wild-type mice after SNI (Fig. 1D and E, 1.32 ± 0.05, n = 23-38 slices from 3 mice, $p < 0.05$), whereas there was no significant difference between the intensity before and that 7 days after SNI in the Y1472F-KI mice (Fig. 1D and E, naive: 0.92 ± 0.04 vs. SNI: 0.88 ± 0.04, n = 31 slices from 3 mice). These results suggest that protein expression of BEGAIN in the spinal dorsal horn was affected (i.e., increased) by the phosphorylation of GluN2B at Y1472 in the spinal dorsal horn after peripheral nerve injury.

Generation of BEGAIN knockout mouse

To clarify the role of BEGAIN in pain transmission after peripheral nerve injury, we generated its knockout (KO) mice. The targeting vector construct was designed as shown in Fig. 2A. Homologous recombination in ES cells was confirmed by Southern blot analysis (Fig. 2B). BEGAIN$^{flox/+}$ mice were crossed with TLCN-Cre mice (Nakamura et al., 2001, Fuse et al., 2004), and BEGAIN $^{-/+}$ mice were further interbred to generate BEGAIN$^{-/-}$ mice (BEGAIN-KO). BEGAIN-KO mice showed the normal Mendelian ratio of offspring (1: 2.06: 0.98 based on 657 mice; Table 2) following breeding of BEGAIN$^{-/+}$ mice. BEGAIN deletion in the spinal dorsal horn and DRG was confirmed by RT-PCR using wild-type and BEGAIN-KO mice. BEGAIN mRNA was completely missing in the spinal dorsal horn and DRG in the BEGAIN-KO mice (Fig. 2C). The amount of BEGAIN mRNA in the DRG was much less than that in the spinal dorsal horn, suggesting that the BEGAIN protein in the spinal cord was mainly expressed in spinal cord neurons.

Expression and distribution of BEGAIN in the central nervous system

In a previous study, BEGAIN mRNA was detected in the whole brain, but not in other tissues, such as heart, spleen, lung, liver, kidney, skeletal muscles, and testis (Deguchi et al., 1998). However, its expression in the spinal cord had not been clarified. By RT-PCR, we analyzed the expression in the spinal cord and brain during postnatal development, because we detected it in the spinal dorsal horn for the first time in this

report. The expression was maintained at a nearly equal level during the postnatal development stages from day 0 to day 56 (Fig. 3A). We next analyzed the distribution of BEGAIN protein in adult mice by performing Western blotting. Mouse BEGAIN is comprised of 600 amino acids (Accession No. Q68EF6), and it was found to have a molecular mass of 65 kDa by Western blotting (Fig. 3B, arrowhead). Since the band was observed in the spinal dorsal horn, but not in the ventral horn (Fig. 3), it seemed that BEGAIN was involved in sensory transmission, but not in motor neuron functions. On the other hand, BEGAIN was strongly detected in the cortex and hippocampus, but not in the cerebellum and medulla oblongata (Fig. 3B, WT). Thus, in our Western blot analysis, BEGAIN was expressed in the spinal dorsal horn and restricted regions in the brain, which expression was lost in the BEGAIN-KO mice (Fig. 3B, BEG-KO).

Concentration of BEGAIN at the synapse in spinal lamina II

The spinal dorsal horn is organized into laminae I-VI, where peripheral inputs are received from different types of fibers: Aβ, Aδ, and C (Rexed, 1952). To clarify the participation of BEGAIN in abnormal pain transmission, we analyzed the localization of BEGAIN in these laminae by performing immunohistochemistry using anti-BEGAIN antibody. BEGAIN was detected in the superficial area of the spinal dorsal horn in wild-type mice, but not in that in BEGAIN-KO mice (Fig. 4A). BEGAIN was co-localized with an IB4 lectin-binding non-peptidergic population (Fig. 4Ba and e), which lectin targets the dorsal part of lamina IIi (Fig. 4C). PKCγ was concentrated in

496 the ventral part of laminae IIi and IIIo (Fig. 4C; (Polgar et al., 1999, Neumann et al.,
497 2008)). BEGAIN was highly concentrated in the IB4-positive area (Fig. 4Bd and e);
498 however, its signal was also detected in the PKCγ-positive area (Fig. 4Dd and e,
499 arrowheads), where myelinated fibers terminate (Fig. 4C). These results indicate that
500 BEGAIN positive neurons may receive not only nociceptive but also innocuous stimuli
501 from primary afferent fibers. On the other hand, the localization of IB4 and PKCγ in the
502 spinal dorsal horn was not affected in BEGAIN-KO mice as compared with wild-type
503 mice (Fig. 4Bb, Db and E).

504 To determine the lamina specificity of (SNI-induced) BEGAIN up-regulation
505 inside the spinal lamina IIi, we measured the fluorescence intensity of BEGAIN signals
506 in PKCγ-positive and IB4-positive areas in the lamina IIi. We identified a 1.51 ±
507 0.03-fold and 1.49-fold ± 0.03 increase (both $p < 0.05$) in the BEGAIN signals in the
508 respective IB4- and PKCγ-positive areas of the spinal dorsal horn after SNI (Fig. 4E and
509 F; n = 31-39 slices from 3 mice). These results indicate that BEGAIN up-regulation
510 was broadly distributed in lamina IIi. Also, no BEGAIN signals were detected in
511 SNI-operated BEGAIN-KO mice (Fig. 4E)

512 To clarify the localization of BEGAIN at synapses, we immunostained for
513 BEGAIN and for PSD-95 and synaptophysin, which are markers for post- and
514 pre-synapses, respectively. BEGAIN was detected in PSD-95- (Fig. 5Aa1-a3, arrows)
515 and synaptophysin-positive (Fig. 5Ac1–c3, arrows) sites in spinal lamina IIi. On the
516 other hand, it was not detected in GFAP-positive cells, i.e., astrocytes (Fig. 5Ad1–d3,

arrowheads). To confirm the co-localization of BEGAIN and PSD-95 or synaptophysin, we performed Manders' overlap coefficient analysis. The fluorescent signals of BEGAIN reliably overlapped with PSD-95 and synaptophysin, but not with GFAP (Fig. 5Ae, Manders' overlap coefficient 0.71 ± 0.01, 0.50 ± 0.02, and 0.13 ± 0.02, respectively). These results indicate that BEGAIN localized at the synapse in the spinal lamina IIi. To further confirm the distribution of BEGAIN at the synapse of the spinal dorsal horn, we separated 6 fractions from the spinal dorsal horn biochemically. PSD-95 and GluN2B were highly enriched in the crude PSD (cPSD) fraction in both wild-type and BEGAIN-KO mice (Fig. 5B). BEGAIN was detected in the homogenate, P1, P2, and cPSD, but not in soluble fractions, S1 and S2. BEGAIN was highly enriched in the cPSD fraction of the spinal dorsal horn (Fig. 5B, upper panel). The subcellular distribution pattern of BEGAIN in the hippocampus was similar to that in the spinal dorsal horn (Fig. 5B). These results and those shown in Figure 4 suggest that BEGAIN is a synaptic protein in neurons of the spinal lamina IIi. Furthermore, BEGAIN might be a postsynaptic protein, because BEGAIN was abundant in the PSD fraction and Manders' overlap coefficient for PSD-95 was higher than that for synaptophysin. On the other hand, BEGAIN was not detected in P2 and cPSD in BEGAIN-KO mice, whereas PSD-95 and GluN2B were detected in them (Fig. 5B, BEG-KO).

EPSC kinetics in lamina II of spinal dorsal horn after SNI in wild-type and BEGAIN-KO mice after SNI

538 To clarify the role of BEGAIN in the channel activity of spinal lamina II neurons
539 after SNI, we analyzed spontaneous EPSCs and evoked EPSCs mediated by AMPA
540 receptor (AMPAR) and NMDAR in the substantia gelatinosa (SG) neurons of lamina II
541 (Fig. 6). Whole-cell recordings were obtained from 18 and 17 SG neurons in
542 SNI-operated wild-type mice and BEGAIN-KO ones, respectively. There was no
543 difference in input membrane resistance (WT, 362 ± 66 MΩ, n = 9; KO, 405 ± 71 MΩ, n
544 = 11; $P > 0.05$) or membrane capacitance (WT, 61.1 ± 5.6 pF, n = 9; KO, 63.8 ± 8.0 pF, n
545 = 11; $P > 0.05$) between wild-type and BEGAIN-KO mice. Under the voltage-clamp
546 condition at a holding potential of -70 mV, SG neurons examined in both mice exhibited
547 spontaneous EPSCs. The amplitude and frequency of spontaneous EPSCs did not differ
548 between the 2 groups of mice (frequency, 11.0 ± 2.2 Hz (n = 10) in WT, 11.6 ± 2.0 Hz (n
549 = 11) in KO, $P > 0.05$; amplitude, 11.4 ± 1.5 pA (n = 10) in WT, 11.3 ± 1.2 pA (n = 11) in
550 KO, $P > 0.05$). These results suggest that BEGAIN knockdown did not alter passive
551 membrane properties or spontaneous excitatory synaptic transmission of SG neurons.
552 We then examined evoked excitatory synaptic responses by focal stimulation. The
553 amplitude of evoked EPSCs also did not differ between the 2 groups (WT, 173 ± 60 pA, n
554 = 9; KO, 319 ± 155 pA, n = 6; $P > 0.05$) recorded at a holding potential of -70 mV. In
555 the presence of a $GABA_A$ receptor antagonist, bicuculline (20 μM); a glycine receptor
556 antagonist, strychnine (2 μM); or a non-NMDA receptor antagonist, CNQX (20 μM), the
557 evoked EPSCs were completely inhibited, indicating that the evoked EPSCs were
558 mediated by AMPA receptors. We further examined evoked NMDAR-EPSCs isolated in

559 the presence of these 3 antagonists at a holding potential of +40 mV, as previously
560 reported (Katano et al., 2008). The NMDAR-EPSCs in BEGAIN-KO mice had a
561 different shape of currents in comparison with those in wild-type mice. The former
562 mice showed relatively slower developing currents and did not have the normal rising
563 phase (left and middle traces in Fig. 6A). Also, the time to the peak of NMDAR-EPSCs
564 in BEGAIN-KO mice was significantly longer than that in wild-type mice. However,
565 the time to the peak and decay time of AMPA-EPSCs (evoked EPSCs recorded at -70
566 mV) did not differ between wild-type and BEGAIN-KO mice (the left graph in Fig. 6B).
567 The delay between times to peak for AMPAR- and NMDAR-EPSCs elicited in singe SG
568 neurons was also longer in BEGAIN-KO mice than in wild-type mice (the right graph in
569 Fig. 6B). The amplitude of NMDAR-EPSCs and the ratio of NMDAR- to
570 AMPAR-EPSCs amplitude did not differ between wild-type and BEGAIN-KO mice (Fig.
571 6C). These results indicate that slower developing NMDAR-EPSCs in the
572 BEGAIN-KO mice resulted in lengthening of the delay between times to peak for
573 AMPAR- and NMDAR-EPSCs.
574
575 **Attenuation of mechanical allodynia in BEGAIN-KO mice after SNI**
576 To examine behavioral consequences of altered NMDAR-EPSCs in BEGAIN-KO
577 mice, we next assessed mechanical sensitivity of the mice after SNI. In naive mice,
578 there was no significant difference in the withdrawal threshold to mechanical (WT: 1.02
579 ± 0.06 g, n = 12; BEGAIN-KO: 1.09 ± 0.11 g, n = 13) stimuli between wild-type and

BEGAIN-KO mice, suggesting that BEGAIN was not involved in nociception in naive mice (Fig. 7A). Since thermal allodynia was not observed in the SNI model (Decosterd and Woolf, 2000), we examined the effects of BEGAIN knock-down on the mechanical sensitivity. Following the SNI operation, the paw withdrawal threshold of both wild-type and BEGAIN-KO mice markedly dropped on day 3, but the threshold in the BEGAIN-KO mice was significantly higher than that in the wild-type mice (Fig. 7B, WT: 0.29 ± 0.07 g, n = 11; BEGAIN-KO: 0.63 ± 0.11 g, n = 14). The decreased threshold in each group was maintained after day 7 (WT: 0.32 ± 0.10 g, n = 11; BEGAIN-KO: 0.56 ± 0.08 g, n = 14), and was retained over the 40-day observation period after SNI (WT: 0.27 ± 0.11 g, n = 11 and BEGAIN-KO: 0.78 ± 0.15 g, n = 14). The decrease in the mechanical threshold was significantly attenuated in BEGAIN-KO mice as compared with that in the wild-type mice after SNI. Collectively, these results suggest that BEGAIN was involved in neuropathic pain after peripheral nerve injury.

Discussion

Comparative analysis of PSD fraction of spinal dorsal horn by iTRAQ-based proteomic approach using Y1472F-KI mice before and after SNI

To screen for neuropathic pain-related proteins in the signaling pathway following the phosphorylation of GluN2B at its Y1472, we performed a comparative proteomic analysis using the PSD fraction. From this analysis, we identified 271 PSD proteins, including glutamate receptors, associated signaling proteins, and scaffold proteins. Thirteen proteins were specifically increased in expression in the wild-type SNI among the 4 groups (Fig. 1C, Table 1 and PASS00929 in Peptide Atlas), indicating that their accumulation to the PSD after SNI depends on the phosphorylation of GluN2B at Y1472. Since calcium influx is attenuated in Y1472F-KI mice (Nakazawa et al., 2006, Matsumura et al., 2010, Katano et al., 2011), it is possible that the increase in expression of these 13 proteins, such as CaMKIIβ, Disk large-associated protein 3 (SAPAP 3), and BEGAIN, depended on the intracellular calcium signaling after SNI. The binding of CaMKII to GluN2B in the synapse is facilitated by autophosphorylated CaMKII (Bayer and Schulman, 2001, Bayer et al., 2006), which requires calcium influx from GluN2B-containing NMDAR (Abe et al., 2005, Nakazawa et al., 2006, Thalhammer et al., 2006, Matsumura et al., 2010, Halt et al., 2012). Activated CaMKIIβ, with activation due to calcium influx, phosphorylates SAPAP, thereby inducing its accumulation at the synapse (Shin et al., 2012). Also, SAPAP is necessary for the recruitment of BEGAIN to PSDs via binding to PSD-95 (Deguchi et al., 1998).

In our proteomic analysis Protein piccolo and SynGAP were increased in amount in both wild-type and Y1472F-KI mice after SNI (Table 1), suggesting that accumulation of these proteins in the PSD during neuropathic pain did not require the phosphorylation of GluN2B at its Y1472. Our proteomic analysis using Y1472F-KI mice is an effective design for identification of chronic pain-related proteins in either the phosphorylation-dependent or -independent pathways.

Identification of BEGAIN as a neuropathic pain related-protein in the spinal dorsal horn

Among candidate proteins in our proteomic analysis, we focused on BEGAIN, because it specifically increased in wild-type SNI mice (Table 1 and Fig. 1D and E) and, furthermore, because its role had not been clarified. BEGAIN was originally identified as a binding protein of PSD-95; and it was shown to be specifically expressed in brain and to be abundant in the PSD fraction (Deguchi et al., 1998, Lim et al., 2003). Our proteomic study supports the possibility that following phosphorylation of GluN2B at Y1472, BEGAIN is transferred to the NMDAR complex of the spinal dorsal horn after peripheral nerve injury; because protein up-regulation of BEGAIN in the PSD after SNI was affected by the phosphorylation of GluN2B at Y1472. On the other hand, BEGAIN is transferred to the Triton X-100-insoluble fraction, which is similar to the cPSD fraction, via binding of PSD-95 in Chinese hamster ovary cells; and its localization at the synapse is decreased by inhibition of NMDAR in cultured hippocampus neurons (Deguchi et al.,

1998, Yao et al., 2002). It is assumed that localization of BEGAIN, as a part of the NMDAR complex, is influenced by activation of NMDARs (Lim et al., 2003). In our present study, mechanical allodynia after SNI was significantly attenuated in the BEGAIN-KO mice. Therefore, we consider that BEGAIN was required for the activities of NMDARs after peripheral nerve injury with the phosphorylation of GluN2B in the spinal dorsal horn. Moreover, BEGAIN and GluN2B were highly enriched in the cPSD not only in the spinal dorsal horn, but also in the hippocampus (Fig. 3B), raising the possibility that BEGAIN is also involved in learning and memory following the phosphorylation of GluN2B at its Y1472 in the hippocampus.

Modulation of EPSCs of NMDAR by BEGAIN in spinal lamina II after peripheral nerve injury

Precise control of NMDAR-EPSC kinetics is crucial for the maintenance of neural plasticity during neuropathic pain as well as during learning and memory formation (Paoletti et al., 2013). Alterations of NMDAR-EPSCs in lamina II neurons, i.e., a slower decay phase of currents were earlier demonstrated during hyperalgesia and allodynia following sciatic nerve ligation (Iwata et al., 2007). Interestingly, BEGAIN knock down exhibited slower developing NMDAR- but not AMPAR-EPSCs in spinal lamina II, which prolonged the time to peak between NMDAR- and AMPAR-EPSCs (Fig. 6A and B). NMDAR is well known to have a voltage-dependent Mg^{2+} block, and therefore its activation is needed for simultaneous activation of AMPAR. The relatively

longer delay between times to peak for AMPAR and NMDAR in BEGAIN-KO mice may have caused a reduction in the number of activated NMDARs during glutamatergic synaptic events in SG neurons. It is possible that the attenuated allodynia in the BEGAIN-KO mice was caused by the difference in kinetics of NMDAR-EPSC. It is generally assumed that ligand-binding properties and gating are determined by the GluN2 subunit composition (Paoletti et al., 2013, Glasgow et al., 2014). Iwata et al. (2007) demonstrated that the expression of GluN2B in neurons in spinal lamina II is increased by sciatic nerve ligation. However, our proteomic analysis showed that the amount of GluN2A, B, and D subunits in the PSD was not increased following SNI (PASS00929 in Peptide Atlas), suggesting that the altered NMDAR-EPSCs kinetics in the BEGAIN-KO mice was not due to the GluN2 subunit composition. On the other hand, NMDAR current showed high fluctuation in BEGAIN-KO mice. BEGAIN is localized at the synapse and directly binds to PSD-95 (Deguchi et al., 1998). Thus, NMDAR current might show high fluctuation by destabilization of the PSD complex containing NMDAR or due to higher heterogeneity of the involved channel populations or to a reduction in open probability as a consequence of BEGAIN deletion.

Involvement of BEGAIN in pathological pain in spinal lamina IIi

The current study revealed that BEGAIN was specifically involved in the transmission of abnormal pain, such as allodynia, but not in that of physiological pain (Fig. 7). Interestingly, BEGAIN was detected at synapses of PKCγ-positive as well as

IB4-positive spinal lamina IIi areas (Fig. 4B and C). Generally, PKCγ-positive interneurons receive innocuous stimuli via myelinated fibers in the ventral region of lamina IIi and lamina IIIo (Polgar et al., 1999, Braz et al., 2014); however, during allodynia, the activation of sensory fibers, which normally detect touch, elicits abnormal pain via projection neurons of lamina I through the somatostatin- or PKCγ-positive interneurons in laminae IIi-IV (Torsney and MacDermott, 2006, Neumann et al., 2008, Woolf, 2011, Duan et al., 2014, Peirs et al., 2015). Thus, allodynia is maintained by not only laminae I-IIo but also lamina IIi-IV in the spinal dorsal horn circuits (Neumann et al., 2008, Braz et al., 2014, Duan et al., 2014). Our results and previous studies suggest that BEGAIN serves the abnormal pain transmission in lamina IIi via low-threshold myelinated fibers.

Our findings suggest that NMDAR and BEGAIN mutually interacted for the maintenance of pathological pain in spinal lamina IIi; because BEGAIN expression in the PSD was increased by NMDAR activity accompanying the phosphorylation of GluN2B at Y1472 after peripheral nerve injury (Table 1), and also because BEGAIN modulated the EPSCs of NMDAR (Fig. 6). Accordingly, the pathological pain circuit in the spinal dorsal horn may be established by the regulatory relationship between NMDAR and BEGAIN. Moreover, BEGAIN knock down might have led to destabilization of the PSD complex containing NMDAR, suggesting that BEGAIN, through interaction with PSD-95, stabilized the PSD complex. In addition, the N-terminal sequence of BEGAIN includes a part of the F-BAR (FES-CIP4 Homology and Bin/Amphiphysin/Rvs)

698 homology region, which plays critical roles in membrane reorganization via direct
699 binding to cellular membranes (Frost et al., 2009). After the accumulation of BEGAIN
700 at synapses during the neuropathic pain following NMDAR activation, it would seem that
701 BEGAIN may play a role in neural plasticity via its binding to cellular membranes or
702 formation of the PSD complex. Clarification of the molecular function or modifications
703 of BEGAIN in detail may provide us a better understanding of the mechanism for
704 pathological pain in the spinal dorsal horn.

References

Abe T, Matsumura S, Katano T, Mabuchi T, Takagi K, Xu L, Yamamoto A, Hattori K, Yagi T, Watanabe M, Nakazawa T, Yamamoto T, Mishina M, Nakai Y, Ito S (2005) Fyn kinase-mediated phosphorylation of NMDA receptor NR2B subunit at Tyr1472 is essential for maintenance of neuropathic pain. Eur J Neurosci 22:1445-1454.

Bayer KU, LeBel E, McDonald GL, O'Leary H, Schulman H, De Koninck P (2006) Transition from reversible to persistent binding of CaMKII to postsynaptic sites and NR2B. J Neurosci 26:1164-1174.

Bayer KU, Schulman H (2001) Regulation of signal transduction by protein targeting: the case for CaMKII. Biochem Biophys Res Commun 289:917-923.

Braz J, Solorzano C, Wang X, Basbaum AI (2014) Transmitting pain and itch messages: a contemporary view of the spinal cord circuits that generate gate control. Neuron 82:522-536.

Carlin RK, Grab DJ, Cohen RS, Siekevitz P (1980) Isolation and characterization of postsynaptic densities from various brain regions: enrichment of different types of postsynaptic densities. J Cell Biol 86:831-845.

Chaplan SR, Bach FW, Pogrel JW, Chung JM, Yaksh TL (1994) Quantitative assessment of tactile allodynia in the rat paw. J Neurosci Methods 53:55-63.

Costes SV, Daelemans D, Cho EH, Dobbin Z, Pavlakis G, Lockett S (2004) Automatic and quantitative measurement of protein-protein colocalization in live cells. Biophys J 86:3993-4003.

Craven SE, Bredt DS (1998) PDZ proteins organize synaptic signaling pathways. Cell 93:495-498.

D'Mello R, Marchand F, Pezet S, McMahon SB, Dickenson AH (2011) Perturbing PSD-95 interactions with NR2B-subtype receptors attenuates spinal nociceptive plasticity and neuropathic pain. Mol Ther 19:1780-1792.

Decosterd I, Woolf CJ (2000) Spared nerve injury: an animal model of persistent peripheral neuropathic pain. Pain 87:149-158.

Deguchi M, Hata Y, Takeuchi M, Ide N, Hirao K, Yao I, Irie M, Toyoda A, Takai Y (1998) BEGAIN (brain-enriched guanylate kinase-associated protein), a novel neuronal PSD-95/SAP90-binding protein. J Biol Chem 273:26269-26272.

Duan B, Cheng L, Bourane S, Britz O, Padilla C, Garcia-Campmany L, Krashes M, Knowlton W, Velasquez T, Ren X, Ross SE, Lowell BB, Wang Y, Goulding M, Ma Q (2014) Identification of spinal circuits transmitting and gating mechanical pain. Cell 159:1417-1432.

Frost A, Unger VM, De Camilli P (2009) The BAR domain superfamily: membrane-molding macromolecules. Cell 137:191-196.

Fuse T, Kanai Y, Kanai-Azuma M, Suzuki M, Nakamura K, Mori H, Hayashi Y, Mishina M (2004) Conditional activation of RhoA suppresses the epithelial to mesenchymal transition at the primitive streak during mouse gastrulation.

Biochem Biophys Res Commun 318:665-672.

Garner CC, Nash J, Huganir RL (2000) PDZ domains in synapse assembly and signalling. Trends Cell Biol 10:274-280.

Glasgow NG, Siegler Retchless B, Johnson JW (2014) Molecular bases of NMDA receptor subtype-dependent properties. J Physiol.

Halt AR, Dallapiazza RF, Zhou Y, Stein IS, Qian H, Juntti S, Wojcik S, Brose N, Silva AJ, Hell JW (2012) CaMKII binding to GluN2B is critical during memory consolidation. EMBO J 31:1203-1216.

Iwata H, Takasusuki T, Yamaguchi S, Hori Y (2007) NMDA receptor 2B subunit-mediated synaptic transmission in the superficial dorsal horn of peripheral nerve-injured neuropathic mice. Brain Res 1135:92-101.

Katano T, Furue H, Okuda-Ashitaka E, Tagaya M, Watanabe M, Yoshimura M, Ito S (2008) N-ethylmaleimide-sensitive fusion protein (NSF) is involved in central sensitization in the spinal cord through GluR2 subunit composition switch after inflammation. Eur J Neurosci 27:3161-3170.

Katano T, Nakazawa T, Nakatsuka T, Watanabe M, Yamamoto T, Ito S (2011) Involvement of spinal phosphorylation cascade of Tyr1472-NR2B, Thr286-CaMKII, and Ser831-GluR1 in neuropathic pain. Neuropharmacology 60:609-616.

Kim Y, Cho HY, Ahn YJ, Kim J, Yoon YW (2012) Effect of NMDA NR2B antagonist on neuropathic pain in two spinal cord injury models. Pain 153:1022-1029.

Lim IA, Merrill MA, Chen Y, Hell JW (2003) Disruption of the NMDA receptor–PSD-95 interaction in hippocampal neurons with no obvious physiological short-term effect. Neuropharmacology 45:738-754.

Luo C, Kuner T, Kuner R (2014) Synaptic plasticity in pathological pain. Trends Neurosci 37:343-355.

Marvizon JC, Perez OA, Song B, Chen W, Bunnett NW, Grady EF, Todd AJ (2007) Calcitonin receptor-like receptor and receptor activity modifying protein 1 in the rat dorsal horn: localization in glutamatergic presynaptic terminals containing opioids and adrenergic alpha2C receptors. Neuroscience 148:250-265.

Matsumura S, Kunori S, Mabuchi T, Katano T, Nakazawa T, Abe T, Watanabe M, Yamamoto T, Okuda-Ashitaka E, Ito S (2010) Impairment of CaMKII activation and attenuation of neuropathic pain in mice lacking NR2B phosphorylated at Tyr1472. Eur J Neurosci 32:798-810.

Mihara Y, Egashira N, Sada H, Kawashiri T, Ushio S, Yano T, Ikesue H, Oishi R (2011) Involvement of spinal NR2B-containing NMDA receptors in oxaliplatin-induced mechanical allodynia in rats. Mol Pain 7:8.

Minami T, Nishihara I, Ito S, Sakamoto K, Hyodo M, Hayaishi O (1995) Nitric oxide mediates allodynia induced by intrathecal administration of prostaglandin E2 or prostaglandin F2 alpha in conscious mice. Pain 61:285-290.

Mishina M, Sakimura K (2007) Conditional gene targeting on the pure C57BL/6 genetic background. Neurosci Res 58:105-112.

788 Nakamura K, Manabe T, Watanabe M, Mamiya T, Ichikawa R, Kiyama Y, Sanbo M, Yagi
789 T, Inoue Y, Nabeshima T, Mori H, Mishina M (2001) Enhancement of
790 hippocampal LTP, reference memory and sensorimotor gating in mutant mice
791 lacking a telencephalon-specific cell adhesion molecule. Eur J Neurosci
792 13:179-189.
793 Nakazawa T, Komai S, Watabe AM, Kiyama Y, Fukaya M, Arima-Yoshida F, Horai R,
794 Sudo K, Ebine K, Delawary M, Goto J, Umemori H, Tezuka T, Iwakura Y,
795 Watanabe M, Yamamoto T, Manabe T (2006) NR2B tyrosine phosphorylation
796 modulates fear learning as well as amygdaloid synaptic plasticity. EMBO J
797 25:2867-2877.
798 Neumann S, Braz JM, Skinner K, Llewellyn-Smith IJ, Basbaum AI (2008) Innocuous,
799 not noxious, input activates PKCgamma interneurons of the spinal dorsal horn via
800 myelinated afferent fibers. J Neurosci 28:7936-7944.
801 Paoletti P, Bellone C, Zhou Q (2013) NMDA receptor subunit diversity: impact on
802 receptor properties, synaptic plasticity and disease. Nat Rev Neurosci 14:383-400.
803 Peirs C, Williams SP, Zhao X, Walsh CE, Gedeon JY, Cagle NE, Goldring AC, Hioki H,
804 Liu Z, Marell PS, Seal RP (2015) Dorsal Horn Circuits for Persistent Mechanical
805 Pain. Neuron 87:797-812.
806 Peng HY, Chen GD, Lai CY, Hsieh MC, Lin TB (2013) Spinal serum-inducible and
807 glucocorticoid-inducible kinase 1 mediates neuropathic pain via kalirin and
808 downstream PSD-95-dependent NR2B phosphorylation in rats. J Neurosci
809 33:5227-5240.
810 Polgar E, Fowler JH, McGill MM, Todd AJ (1999) The types of neuron which contain
811 protein kinase C gamma in rat spinal cord. Brain Res 833:71-80.
812 Rexed B (1952) The cytoarchitectonic organization of the spinal cord in the cat. J Comp
813 Neurol 96:414-495.
814 Shilov IV, Seymour SL, Patel AA, Loboda A, Tang WH, Keating SP, Hunter CL,
815 Nuwaysir LM, Schaeffer DA (2007) The Paragon Algorithm, a next generation
816 search engine that uses sequence temperature values and feature probabilities to
817 identify peptides from tandem mass spectra. Mol Cell Proteomics 6:1638-1655.
818 Shin SM, Zhang N, Hansen J, Gerges NZ, Pak DT, Sheng M, Lee SH (2012) GKAP
819 orchestrates activity-dependent postsynaptic protein remodeling and homeostatic
820 scaling. Nat Neurosci 15:1655-1666.
821 Tal M, Bennett GJ (1994) Extra-territorial pain in rats with a peripheral mononeuropathy:
822 mechano-hyperalgesia and mechano-allodynia in the territory of an uninjured
823 nerve. Pain 57:375-382.
824 Tao F, Tao YX, Gonzalez JA, Fang M, Mao P, Johns RA (2001) Knockdown of
825 PSD-95/SAP90 delays the development of neuropathic pain in rats. Neuroreport
826 12:3251-3255.
827 Tao YX, Rumbaugh G, Wang GD, Petralia RS, Zhao C, Kauer FW, Tao F, Zhuo M,
828 Wenthold RJ, Raja SN, Huganir RL, Bredt DS, Johns RA (2003) Impaired NMDA
829 receptor-mediated postsynaptic function and blunted NMDA receptor-dependent

persistent pain in mice lacking postsynaptic density-93 protein. J Neurosci 23:6703-6712.

Thalhammer A, Rudhard Y, Tigaret CM, Volynski KE, Rusakov DA, Schoepfer R (2006) CaMKII translocation requires local NMDA receptor-mediated Ca2+ signaling. EMBO J 25:5873-5883.

Todd AJ (2010) Neuronal circuitry for pain processing in the dorsal horn. Nature Reviews Neuroscience 11:823-836.

Torsney C, MacDermott AB (2006) Disinhibition opens the gate to pathological pain signaling in superficial neurokinin 1 receptor-expressing neurons in rat spinal cord. J Neurosci 26:1833-1843.

Uta D, Furue H, Pickering AE, Rashid MH, Mizuguchi-Takase H, Katafuchi T, Imoto K, Yoshimura M (2010) TRPA1-expressing primary afferents synapse with a morphologically identified subclass of substantia gelatinosa neurons in the adult rat spinal cord. Eur J Neurosci 31:1960-1973.

Woolf CJ (2011) Central sensitization: implications for the diagnosis and treatment of pain. Pain 152:S2-15.

Yao I, Iida J, Nishimura W, Hata Y (2002) Synaptic and nuclear localization of brain-enriched guanylate kinase-associated protein. J Neurosci 22:5354-5364.

Figure legends

Figure 1. Behavioral analysis and identification of BEGAIN as a neuropathic pain-related protein in the postsynaptic density (PSD) fraction.

(A) Attenuation of mechanical allodynia by inhibition of NMDAR containing GluN2B. Withdrawal thresholds of wild-type and Y1472F-KI (YF-KI) mice were assessed before and 7 days after SNI by use of von Frey filaments. The effect of the GluN2B antagonist Ro 25-6981 (100 μg / mouse) 7 days after SNI mice was assessed and measurements were repeated 3 times within 30 and 90 min after *i.t.* injection of Ro 25-6981 at an interval of at least 15 min. The average was used as the value of the withdrawal threshold. Data are expressed as the mean ± SEM, n = 12. Significant differences are indicated: Mann-Whitney U-test, *$p < 0.05$, **$p < 0.01$ *vs*. naive mice; #$p < 0.01$ *vs.* WT SNI mice. (B) Purity of PSD fraction. PSD fractions were purified by sucrose-density gradient centrifugation and analyzed by Western blotting with anti-PSD-95 and anti-Hsp60 antibodies. PSD-95 is a marker protein of the PSD (upper panel); and Hsp60, one for mitochondria (lower panel), as described in "Material and Methods." (C) SDS-PAGE of PSD fractions and work flow for quantitative proteomics using iTRAQ reagents. PSD fractions of 4 comparison groups were individually separated into 6 parts by 10% SDS-PAGE after CBB staining. Proteins in each gel piece were digested and labeled with 4-plex iTRAQ reagents (114: WT naive / white, 115: WT SNI / magenta, 116: YF-KI naive / gray, and 117: YF-KI SNI / blue). Differentially labeled peptide samples in the same part were combined and subjected to subsequent protein

identification and quantitative analysis. As a result of examination of all six parts, 271 proteins were identified and quantified. (D) Immunohistochemistry of BEGAIN in the spinal dorsal horn before and after SNI. Transverse sections (14 μm) of lumbar spinal cords prepared from WT and Y1472F-KI (YF-KI) mice before (naive) and 7 days after SNI were immunostained with anti-BEGAIN antibody. Higher magnification of the white boxes in the left images is shown as the right images. Scale bars, 50 and 10 μm. (E) Quantification of immunoreactivity of BEGAIN. Immunostaining intensity of WT and YF-KI was measured by using ImageJ. The intensity of immunofluorescence for the wild-type naive mice was taken as "1," and the data are expressed as the mean ± SEM (n = 23-31 slices from 3 mice for each group). Significant differences were determined by Mann-Whitney U-test: *$p < 0.05$ *vs.* WT naive mice, #$p < 0.05$ *vs.* WT SNI mice.

Figure 2. Generation of brain-enriched guanylate kinase-associated protein knockout (BEGAIN-KO) mice.

(A) Knockout strategy for the *begain* gene. Homologous recombination of the targeting plasmid resulted in insertion of the *pgk-neo* cassette (*neo*) and *loxP* sequences (filled triangles) into introns 3 and 5 of the *begain* gene. The floxed mice following germline transmission of ES cells with homologous recombination (Targeted) were crossed with "Cre-deleter" mice. Exons 4 and 5 of the *begain* gene were deleted from the germline (knockout) together with the *neo* cassette. A: Afl II, B: BamH I, H: Hind III (B) Southern blot analysis for homologous recombination of ES cells. Genomic DNA

prepared from the wild-type (+/+) and begain lox/+ ES cells. (Left) Afl II-digested DNA hybridized with a 5'probe: 25.9 kb for wild-type and 10.8 kb for floxed allele. (Middle) BamH I-digested DNA hybridized with a Neo probe: 7.4 kb for floxed allele. (Right) Kpn I- or Afl II-digested DNA hybridized with a 3'probe: 25.9 kb or 8.15 kd, respectively, for wild-type and 16.9 kb or 6.6 kb, respectively, for floxed allele. (C) Expression of BEGAIN. RT-PCR of the spinal dorsal horn and DRG samples from wild-type (WT) and BEGAIN-KO (KO) mice.

Figure 3. Expression of BEGAIN in the central nervous system.

(A) Expression of BEGAIN during in postnatal development. RT-PCR of the spinal cord and brain at postnatal developmental stages between day 0 and day 56. **(B)** Detection of BEGAIN in the central nervous system. Western blot analysis of the central nervous system (30 μg each) in WT and BEGAIN-KO (BEG-KO), performed by use of 10% SDS-PAGE. Results for BEGAIN (arrowhead), PSD-95, and β-tubulin are shown.

Figure 4. Localization of BEGAIN in the spinal dorsal horn.

(A) Detection of BEGAIN in the spinal dorsal horn. Transverse sections (14 μm) of lumbar spinal cords prepared from wild-type (WT, a) and BEGAIN-KO (BEG-KO, b) mice were immunostained with anti-BEGAIN antibody. (B) Double staining of the spinal dorsal horn of wild-type (WT, a, c-e) and BEGAIN-KO (BEG-KO, b) mice by

using anti-BEGAIN antibody and IB4, a marker of non-peptidergic afferents in lamina IIi. "c-e" show high magnification of the white box in "a." Green lines indicate IB4-positive area. Arrowheads indicate BEGAIN single-positive area (d and e). (C) Lamina IIi-IIIo, labeled with IB4 and anti-PKCγ antibody in WT mice (a and b). Higher magnification of the white box in "a" is shown in "b." Green and magenta lines indicate IB4- and PKCγ-positive areas, respectively. (D) Double staining of the spinal dorsal horn of WT (a, c-e) and BEG-KO (b) mice by use of anti-BEGAIN and PKCγ antibodies. Green lines indicate PKCγ-positive area. Arrowheads indicate BEGAIN and PKCγ double-positive area (d and e). (E) Triple staining of the spinal dorsal horn of WT naive, WT SNI and BEG-KO SNI. Green and blue lines indicate IB4- and PKCγ-positive areas, respectively. Scale bars, 50 μm. (F) Quantification of immunostaining intensity of BEGAIN in IB4- and PKCγ-positive areas. The signal of BEGAIN in each area was measured before and after SNI by using ImageJ. The intensity of immunofluorescence for the naive mice was taken as "1," and the data are expressed as the mean ± SEM (n = 31-39 slices from 3 mice for each group). Significant differences, determined by use of Mann-Whitney U-test, are indicated: $*p < 0.05$ *vs*. WT naive mice.

Figure 5. Localization of BEGAIN at the synapses in spinal lamina II.

(A) Double staining of BEGAIN and markers. Transverse sections (14 μm) of lumbar spinal cords were prepared from wild-type (a, c, and d) and BEG-KO (b) mice. BEGAIN (magenta, a-d), PSD-95, a postsynaptic marker (green, a and b), synaptophysin,

presynaptic marker (green, c) and GFAP, an astrocyte marker (green, d) were detected. Higher magnification of the white boxes in "a-d1" is shown in "a-d2." Higher magnification views of the white boxes in "a-d2" are shown in "a-d3 and a-b4". Arrows indicate co-localization signals (a3 and c3), and arrowheads indicate BEGAIN signal without GFAP signals (d3). Scale bars, 50 μm in a-d1 and 10 μm in a-d2 and 3. (e) Quantification of co-localization of BEGAIN with markers made by using Manders' overlap coefficient. (B) Concentration of BEGAIN in cPSD. Western blot analysis of the subcellular fractions of mouse spinal dorsal horn and hippocampus from wild-type (WT) and BEGAIN-KO (BEG-KO) mice. Spinal dorsal horn (10 μg) and hippocampus (7 μg) proteins were incubated with the anti-BEGAIN, anti-GluN2B, anti-PSD-95, and β-tubulin antibodies. Lane H, homogenate; lane P1, nuclear pellet; lane S1, supernatant 1; lane S2, cytosolic synaptosome; lane P2, crude synaptosomal pellet; lane cPSD, crude post synaptic density (0.5% [w/v] Triton X-100-insoluble fraction of P2).

Figure 6. Change in the rising phase of evoked NMDAR-, but not that in AMPAR-EPSCs, in SG neurons of BEGAIN-KO mice.

(A) Examples of evoked AMPAR- and NMDAR-EPSCs in wild-type (WT; left traces) and BEGAIN-KO (BEG-KO; middle traces) mice. NMDAR-EPSCs in KO mice had a slower kinetics than those in WT mice. The EPSC amplitude of the traces was not similar. However, there is no significant differences of the EPSC amplitude between the 2 groups (see Results section). Arrows show peaks for the evoked EPSCs. The right

graph shows normalized summation of current changes of the traces shown in the left and middle traces. Note that delay between the time constants (0.63, indicated by dashed line) for AMPAR- and NMDA-R EPSCs in BEG-KO mice is nearly twice that in WT mice. (B) Summary showing time to peak for AMPAR- and NMDAR-EPSCs (left graph), and delay between times to peak for AMPAR- and NMDAR-EPSCs elicited in single SG neurons (right graph) in WT and BEG-KO mice. (C) Amplitude of evoked EPSCs (left graph) and ratio of NMDAR- to AMPAR-EPSC amplitude (right graph).

Figure 7. Behavioral analysis of wild-type and BEGAIN-KO mice after SNI.

(A) Basal mechanical sensitivity. Withdrawal threshold of naive wild-type (WT, white column) and BEGAIN-KO (BEG-KO, black column) mice was assessed in 8-12-week-old mice. Data are expressed as described in "Material and Methods" as the mean ± SEM (n = 12-13). (B) Time course of paw withdrawal threshold after SNI. Withdrawal thresholds on the ipsilateral side of WT (white circle) and BEG-KO (black circle) mice were assessed before and after SNI. Data are expressed as the mean ± SEM, n = 11 (WT) and 14 (BEG-KO). Significant differences were indicated in Source data.

Table 1. List of proteins whose expression was increased specifically in the wild-type or in both SNI wild type SNI and Y1472F-KI SNI mice.

Expression level of 13 proteins was specifically increased in the wild-type after SNI. Two proteins were increased in both wild-type and Y1472F-KI mice. LowerCI, The

lower bound of the confidence interval for the average ratio; UpperCI, The upper bound of the confidence interval for the average ratio; *, Significant increase.

Table 2. Mendelian ratio of BEGAIN knockout mice.

BEGAIN-KO mice were born at the predicted Mendelian ratio by interbreeding of BEGAIN hetero knockout mice. The ratio was analyzed by use of the chi-square test.

Source data legends

Figure 1-1. Statistical table for behavioral analysis and immunohistochemistry.

(A) Withdrawal threshold after SNI was significantly decreased in both WT and Y1472F-KI mice. In YF-KI and WT with Ro25-6981 after SNI, mechanical allodynia was significantly attenuated. (E) Fluorescence intensity of BEGAIN was specifically increased in the spinal dorsal horn in WT after SNI. Significant difference is indicated in “A” and “E.”

Figure 1-2. Values of Auto Bias for iTRAQ analysis in ProteinPilot.

Observed iTRAQ ratios of all peptides were normalized by using Auto Bias. Gel, a part of gel part in Figure 1C.

Figure 4-1. Statistical table for immunohistochemistry.

(F) Fluorescence intensity of BEGAIN was significantly increased in IB4- and

997 PKCγ-positive areas. Significant difference was indicated in Figure 4F.

998

999 **Figure 7-1. Statistical table.**

1000 (B) Withdrawal threshold at all days after SNI showed a significant difference between

1001 WT and BEG-KO. The withdrawal threshold for WT was significantly decreased at 1

1002 to 42 days after SNI compared with that for WT naive. The withdrawal threshold for

1003 BEG-KO was significantly decreased at 3 to 42 days after SNI compared with that for

1004 BEG-KO naive.

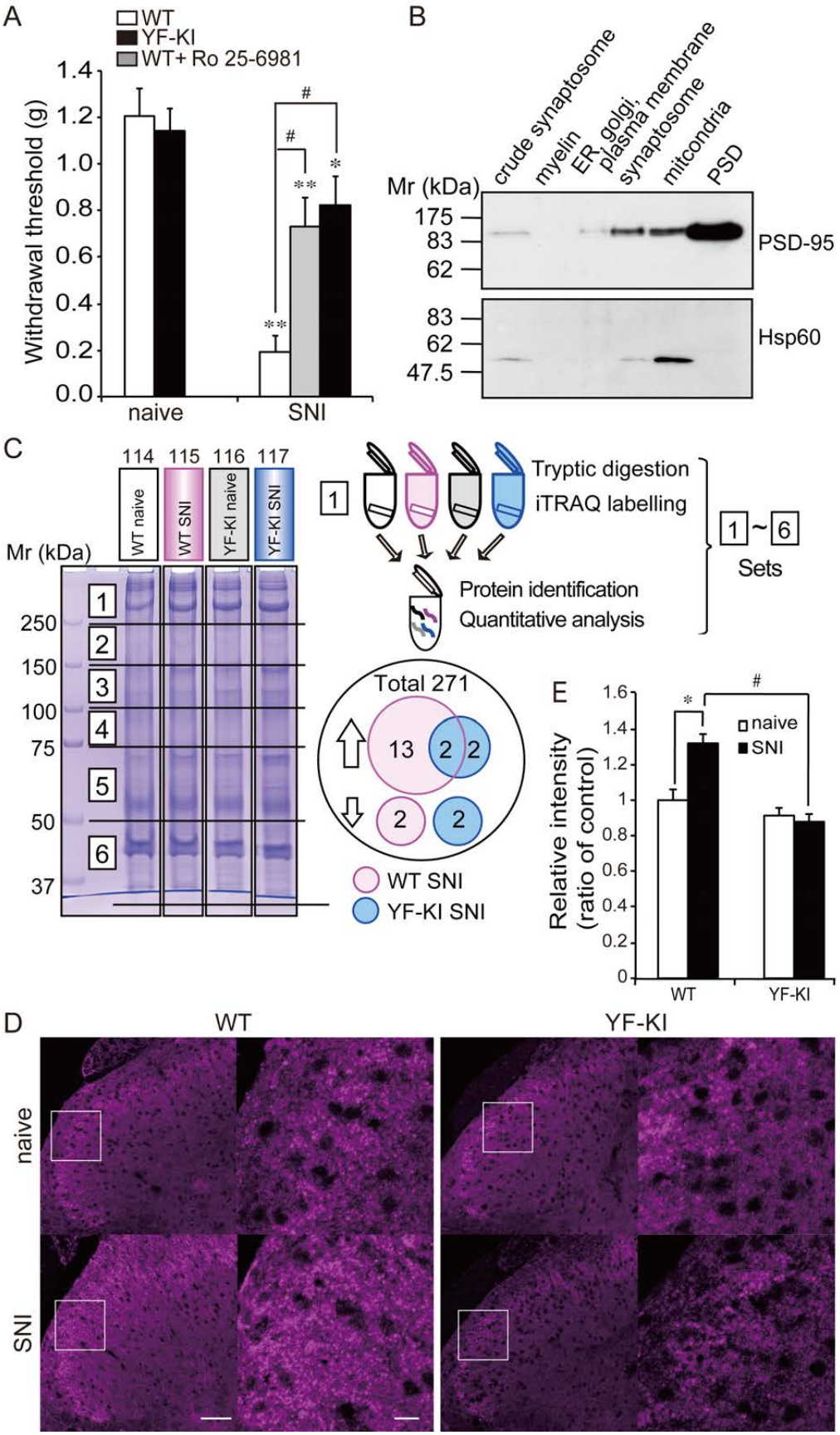

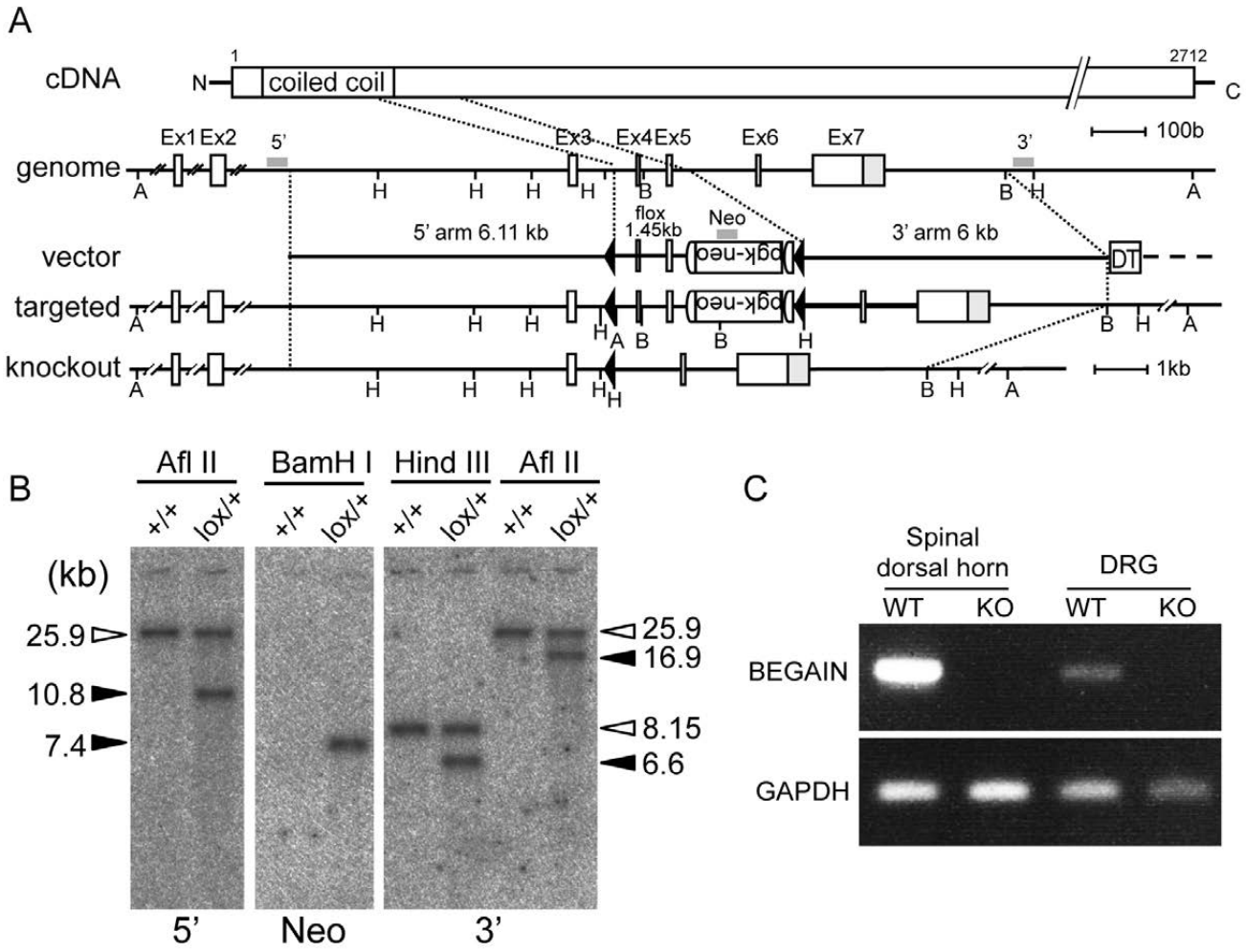

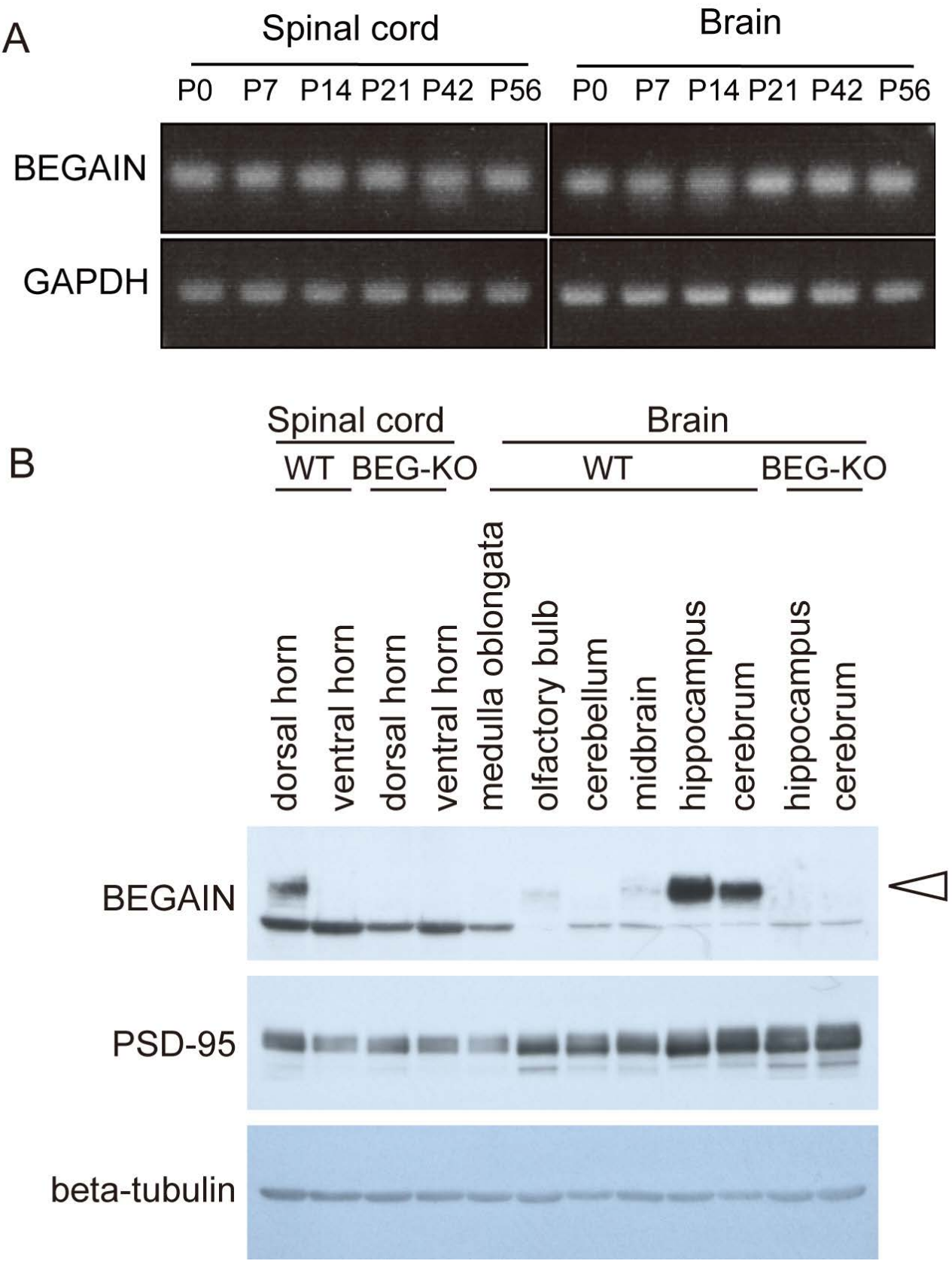

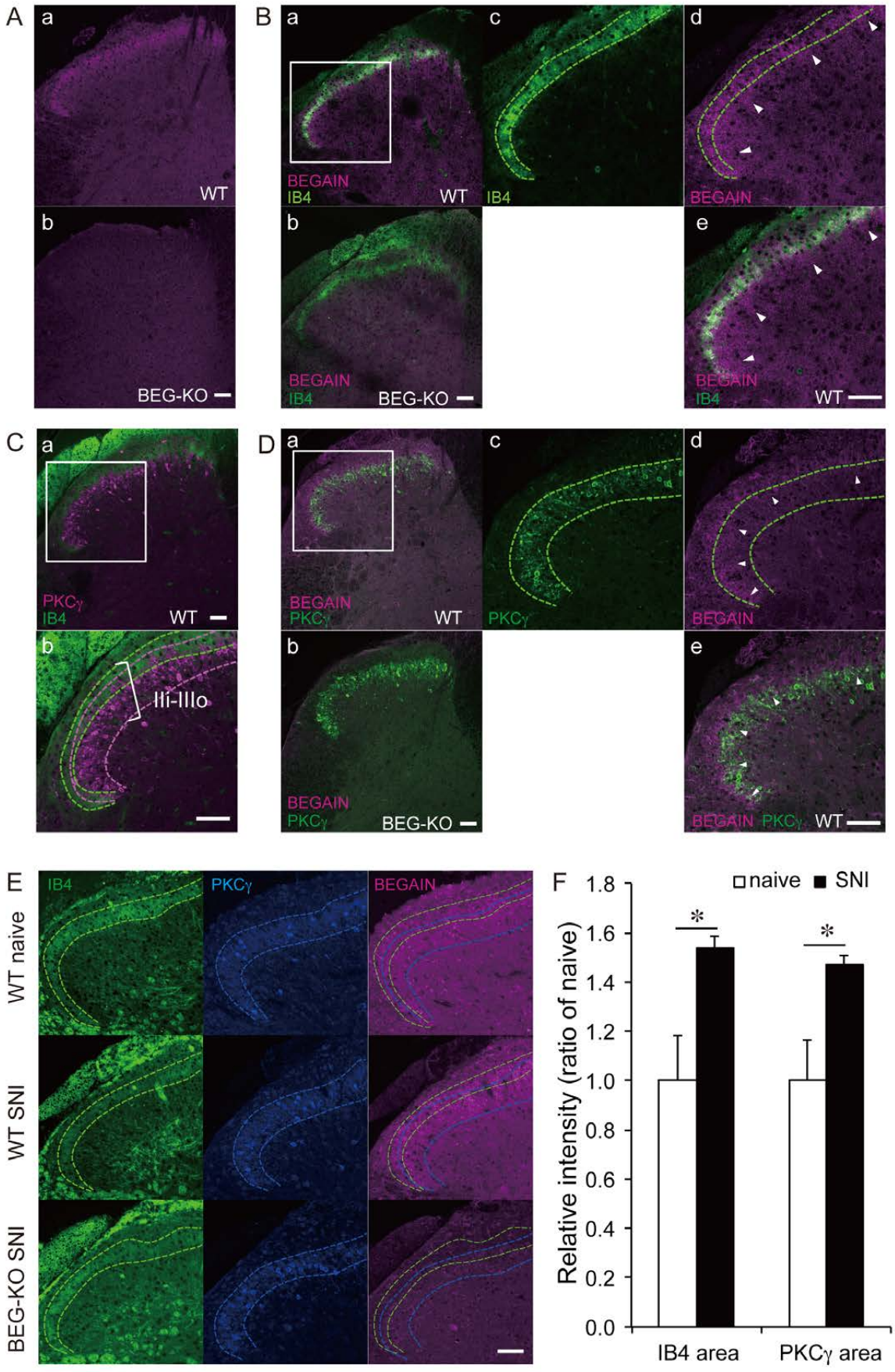

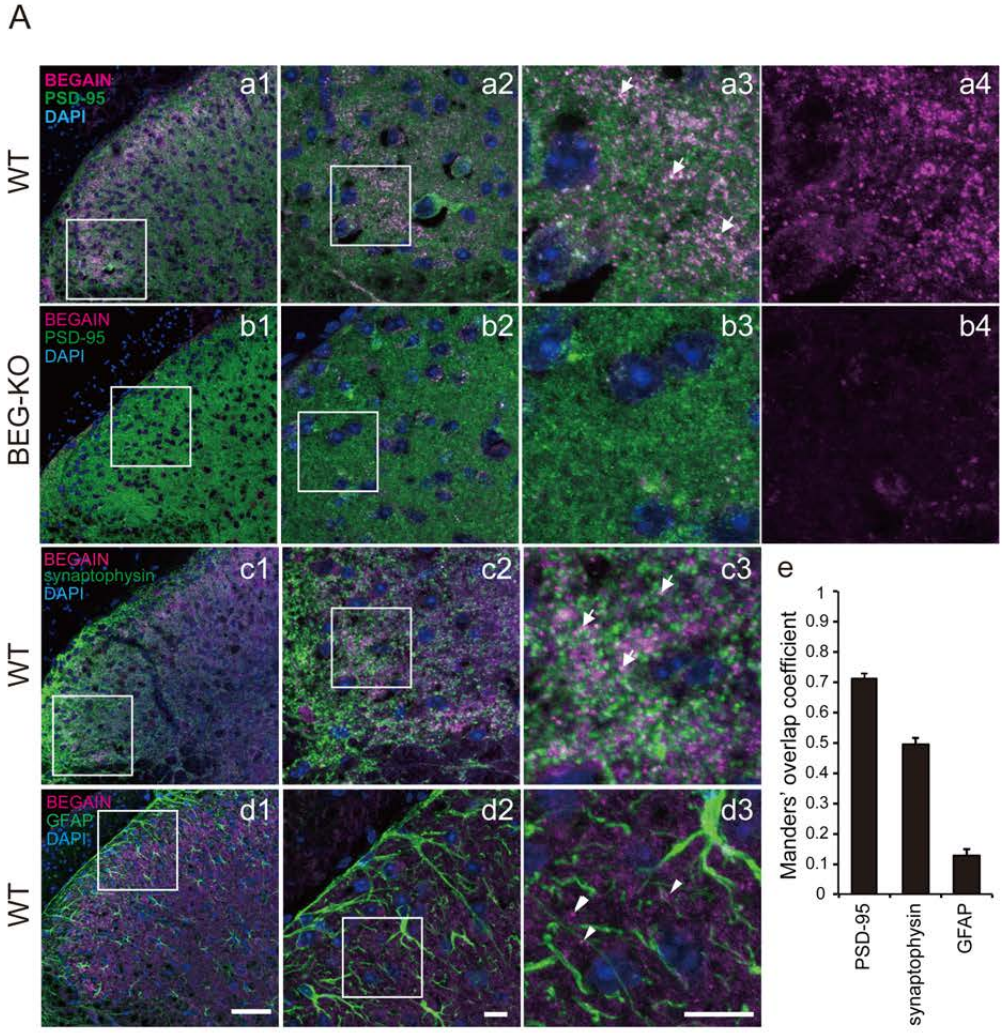

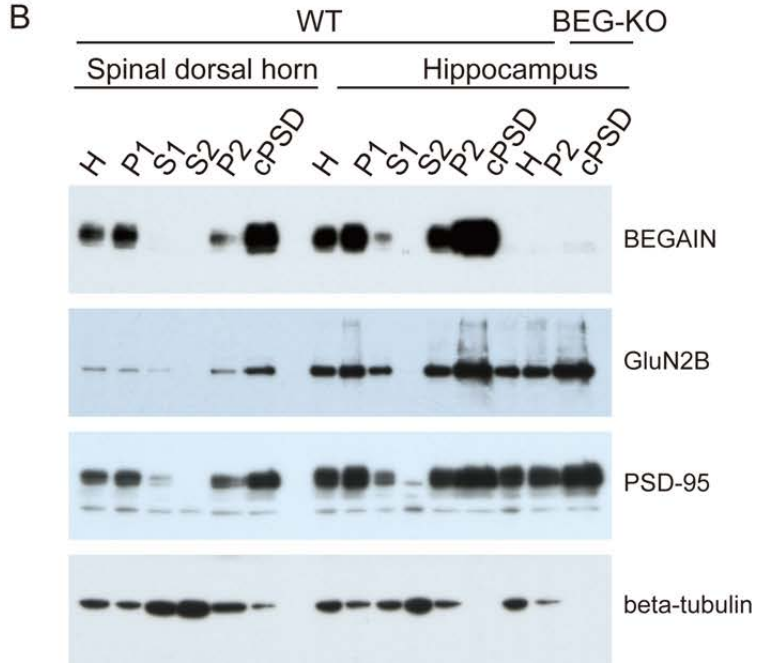

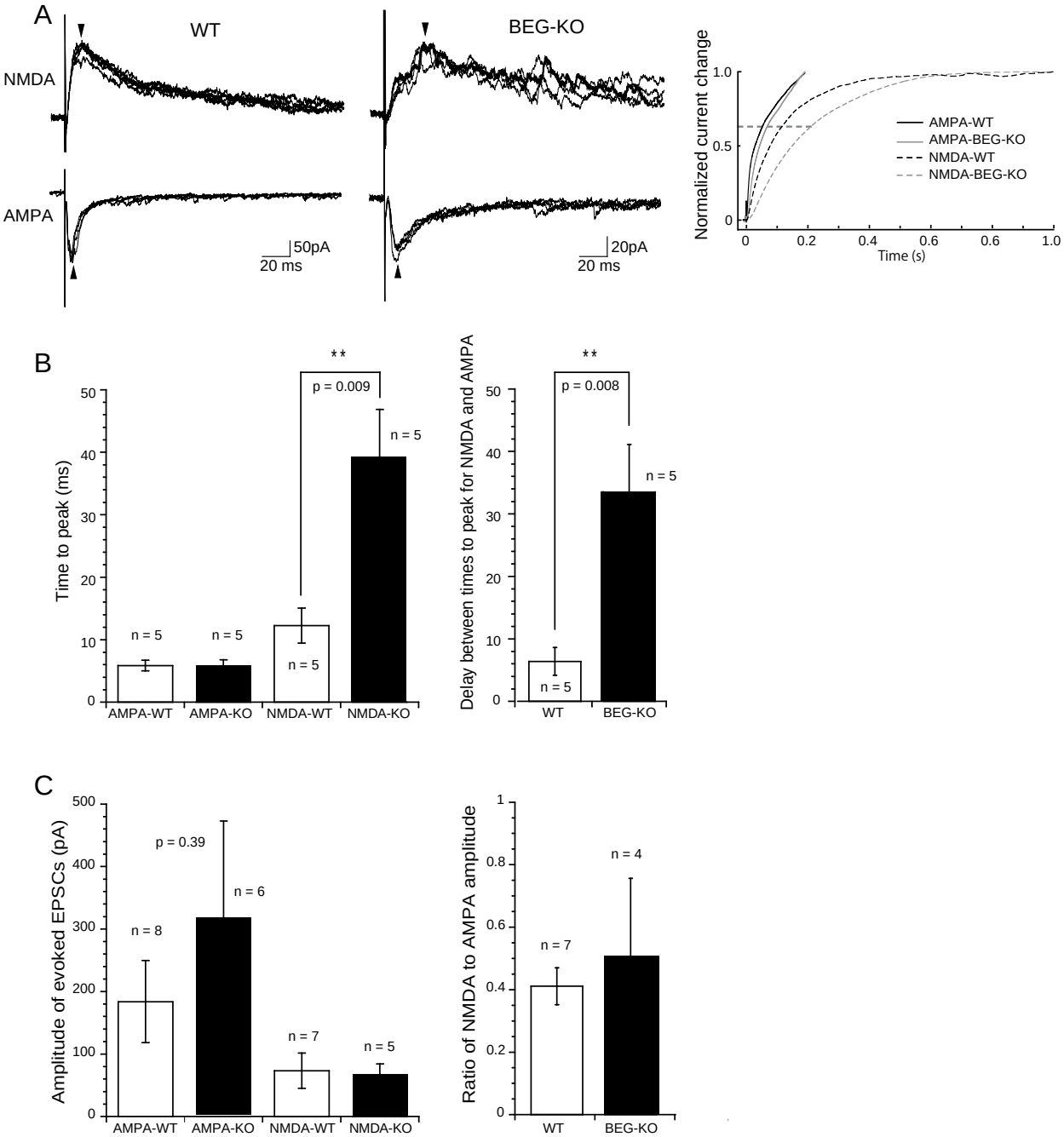

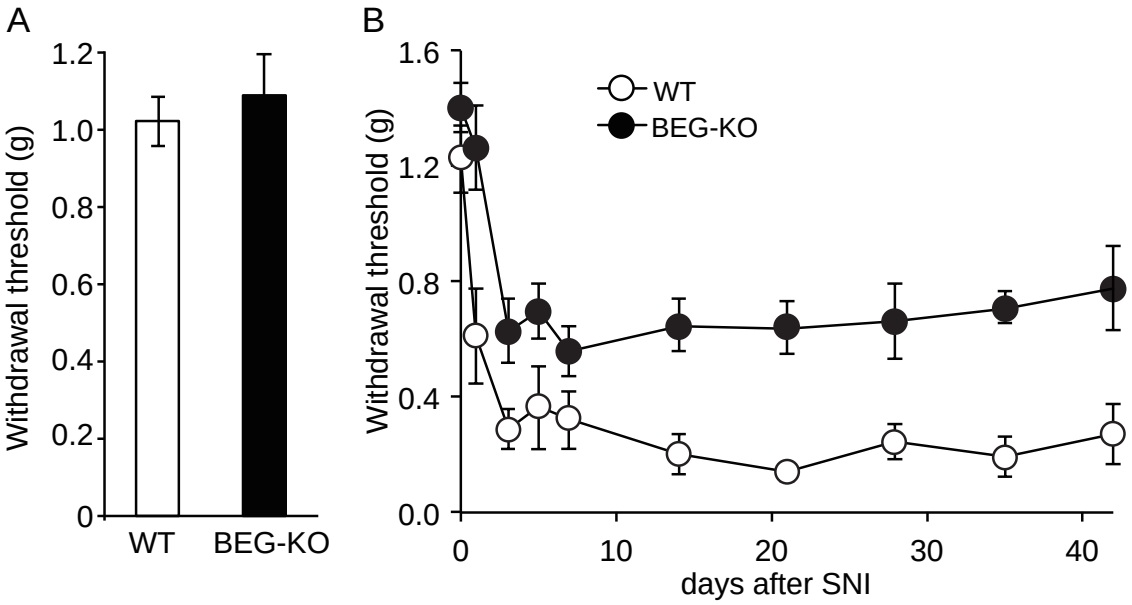

Table 1. List of proteins whose expression was increased specifically in the wild-type or in both SNI wild type SNI and Y1472F-KI SNI mice.

Acsession	Names	115/114		
Q68EF6	Brain-enriched guanylate kinase-associated protein	Ratio	1.3	*
		PVal	0.045	
		Lower CI	1.011	
		Upper CI	1.798	
		117/116		
		Ratio	1.1	
		PVal	0.258	
		Lower CI	0.880	
		Upper CI	1.463	
Acsession	Names	115/114		
P28652	Calcium/calmodulin-dependent protein kinase type II beta chain	Ratio	1.2	*
		PVal	0.031	
		Lower CI	1.018	
		Upper CI	1.385	
		117/116		
		Ratio	1.1	
		PVal	0.067	
		Lower CI	0.990	
		Upper CI	1.283	
Acsession	Names	115/114		
Q923T9	Calcium/calmodulin-dependent protein kinase type II gamma chain	Ratio	1.2	*
		PVal	0.008	
		Lower CI	1.060	
		Upper CI	1.363	
		117/116		
		Ratio	1.1	
		PVal	0.094	
		Lower CI	0.977	
		Upper CI	1.285	
Acsession	Names	115/114		
Q6P9K8	Caskin-1	Ratio	1.6	*
		PVal	0.001	
		Lower CI	1.403	
		Upper CI	1.732	
		117/116		
		Ratio	1.1	
		PVal	0.512	
		Lower CI	0.769	
		Upper CI	1.526	
Acsession	Names	115/114		
Q6PFD5	Disks large-associated protein 3	Ratio	1.2	*
		PVal	0.039	
		Lower CI	1.009	
		Upper CI	1.344	
		117/116		
		Ratio	1.1	
		PVal	0.124	
		Lower CI	0.974	
		Upper CI	1.211	
Acsession	Names	115/114		
P05064	Fructose-bisphosphate aldolase A	Ratio	1.2	*
		PVal	0.011	
		Lower CI	1.046	
		Upper CI	1.317	
		117/116		
		Ratio	1.1	
		PVal	0.364	
		Lower CI	0.920	
		Upper CI	1.230	
Acsession	Names	115/114		
P16858	Glyceraldehyde-3-phosphate dehydrogenase	Ratio	1.3	*
		PVal	0.000	
		Lower CI	1.178	
		Upper CI	1.426	
		117/116		
		Ratio	1.1	
		PVal	0.137	
		Lower CI	0.974	
		Upper CI	1.198	
Acsession	Names	115/114		
P20357	Microtubule-associated protein 2	Ratio	1.194	*
		PVal	0.005	
		Lower CI	1.081	
		Upper CI	1.319	
		117/116		
		Ratio	1.217	
		PVal	0.096	
		Lower CI	0.954	
		Upper CI	1.551	

Acsession	Names	115/114		
P24369	Peptidyl-prolyl cis-trans isomerase B	Ratio	1.265	*
		PVal	0.036	
		Lower CI	1.067	
		Upper CI	1.500	
		117/116		
		Ratio	0.912	
		PVal	0.806	
		Lower CI	0.022	
		Upper CI	38.176	
Acsession	Names	115/114		
P15331	Peripherin	Ratio	1.210	*
		PVal	0.020	
		Lower CI	1.039	
		Upper CI	1.409	
		117/116		
		Ratio	1.085	
		PVal	0.192	
		Lower CI	0.952	
		Upper CI	1.236	
Acsession	Names	115/114		
Q9QYX7	Protein piccolo	Ratio	1.179	*
		PVal	0.010	
		Lower CI	1.046	
		Upper CI	1.328	
		117/116		
		Ratio	1.173	*
		PVal	0.011	
		Lower CI	1.042	
		Upper CI	1.321	
Acsession	Names	115/114		
Q9EQZ6	Rap guanine nucleotide exchange factor 4	Ratio	1.201	*
		PVal	0.003	
		Lower CI	1.087	
		Upper CI	1.326	
		117/116		
		Ratio	1.042	
		PVal	0.464	
		Lower CI	0.922	
		Upper CI	1.177	
Acsession	Names	115/114		
F6SEU4	Ras GTPase-activating protein SynGAP	Ratio	1.194	*
		PVal	0.016	
		Lower CI	1.037	
		Upper CI	1.373	
		117/116		
		Ratio	1.225	*
		PVal	0.002	
		Lower CI	1.088	
		Upper CI	1.381	
Acsession	Names	115/114		
Q64332	Synapsin-2	Ratio	1.4	*
		PVal	1.324	
		LowerCI	1.052	
		Upper CI	1.844	
		117/116		
		Ratio	1.2	
		PVal	2.828	
		LowerCI	0.434	
		Upper CI	3.469	
Acsession	Names	115/114		
P42669	Transcriptional activator protein Pur-alpha	Ratio	1.173	*
		PVal	0.001	
		Lower CI	1.090	
		Upper CI	1.262	
		117/116		
		Ratio	0.873	
		PVal	0.028	
		Lower CI	0.777	
		Upper CI	0.981	

Table 2. Mendelian ratio of BEGAIN knockout mice

	Number	rate	theoretical rate	theoretical value	chi-square test
Total	657				
WT	153	1	1	164.25	
Hetero	330	2.06	2	328.5	
KO	174	0.98	1	164.25	0.50759

Fig.1-1

		Comparison	Mann-Whitney U	n
Fig. 1A	Force (g)	WT naive vs WT SNI	0.0002421	12 mice in one group
		WT naive vs WT SNI + Ro25-6981	0.0102980	
		YF naive vs YF SNI	0.0432658	
		WT SNI vs WT SNI + Ro25-6981	0.0016202	
		WT SNI vs YF SNI	0.0008131	
		YF SNI vs WT SNI + Ro25-6981	0.3042951	
Fig. 1E	Intensity of BEGAIN	WT naive vs WT SNI	0.0487103	23-31 slices from 3 mice in each group
		WT SNI vs YF-KI SNI	0.0487103	

Fig.1-2

Gel	Auto Bias (Median)		
	115/114	116/114	117/114
1	1.3163	1.0467	1.0604
2	1.2254	1.0641	0.8925
3	0.9273	0.9753	1.0206
4	0.7433	1.0111	0.9129
5	0.998	0.9869	0.9197
6	0.9157	0.9237	0.9097

Fig.4-1

		Comparison (WT naive vs WT SNI)	Mann-Whitney U	n
Fig. 4F	Intensity of BEGAIN	In IB4 area	0.0487103	31-39 slices from 3 mice in each group
		In PKCγ area	0.0487103	

Fig.7-1

		Comparison WT vs BEG-KO Mann-Whitney U-test	Comparison naive vs after SNI Bonferroni		
	days after SNI		WT	BEG-KO	
Fig. 7B	0	0.1303			
	1	0.0056	< 0.01		
	3	0.0124	< 0.01	< 0.01	
	5	0.0202	< 0.01	< 0.01	
	7	0.0193	< 0.01	< 0.01	WT: 11mice,
	14	0.0009	< 0.01	< 0.01	BEG-KO: 14 mice
	21	0.0003	< 0.01	< 0.01	
	28	0.0044	< 0.01	< 0.01	
	35	0.0019	< 0.01	< 0.01	
	42	0.0053	< 0.01	< 0.01	
		ANOVA			
	WT	1.36E-18			
	BEG-KO	2.19E-09			